Physics – Uspekhi **47** (9) 923 – 941 (2004)

REVIEWS OF TOPICAL PROBLEMS PACS numbers: **05.45. – a**, **05.65. + b**, 82.40.Bj, 82.40.Ck

Waves and patterns in reaction – diffusion systems. Belousov – Zhabotinsky reaction in water-in-oil microemulsions

V K Vanag

DOI: 10.1070/PU2004v047n09ABEH001742

Contents

Abstract. Advances in nonequilibrium pattern formation in reaction – diffusion systems are reviewed. Special emphasis is placed on patterns found in the spatially extended Belousov – Zhabotinsky reaction dispersed in aerosol OT water-in-oil microemulsions (BZ – AOT system): Turing patterns, packet and standing waves, antispirals and segmented spirals, and accelerating waves and oscillons. All experimental results are explained theoretically and reproduced in computer simulations.

Abbreviations

AOT — OT aerosol (OT is a trade mark), surfactant or SAC
BZ reaction — Belousov – Zhabotinsky reaction
MA — malonic acid
ME — microemulsion
NADPH — nicotinamide adenine dinucleotide phosphate, a biologically active molecule
ODE — ordinary differential equation
SAC — surface-active compound
ferriin — $Fe^{3+}(phen)_3$
ferroin — $Fe^{2+}(phen)_3$
cAMP — cyclic adenosine monophosphate

V K Vanag Department of Chemistry and Volen Center for Complex Systems, Brandeis University,
Waltham, MA 02454, USA
E-mail: vanag@brandeis.edu

Received 18 September 2003, revised 20 December 2003
Uspekhi Fizicheskikh Nauk **174** (9) 991 – 1010 (2004)
Translated by Yu V Morozov; edited by A M Semikhatov

$\det A$ — determinant of a matrix A
0-D, 1-D, 2-D — zero-, one-, and two-dimensional spaces
k_T and k_w — wave numbers corresponding to the $\mathrm{Re}\,\Lambda$ maximum for the Turing instability and wave instability, respectively
$\mathrm{Tr}\,A$ — trace of a matrix A = the sum of the diagonal elements
λ_T — characteristic size of Turing patterns: $\lambda_T = 2\pi/k_T$
λ_w — characteristic size of wave instability: $\lambda_w = 2\pi/k_w$
Λ — eigenvalue of the characteristic equation
$\mathrm{Re}\,\Lambda$ and $\mathrm{Im}\,\Lambda$ — real and imaginary parts of an eigenvalue respectively
$\omega \equiv [H_2O]/[AOT]$
ϕ_d — volume fraction of the dispersed phase (water + surfactant) in a microemulsion
ϕ_w — volume fraction of the aqueous phase in a microemulsion

1. Introduction

Nonlinear dynamics incorporates two closely related large blocks: dynamical systems in a 0-dimensional space (0-D), or point systems described by ordinary differential equations (ODE), and dynamical nonequilibrium patterns in spatially extended systems (1-D, 2-D) described by partial differential equations (3-dimensional patterns remain poorly understood). Most notions developed for 0-D systems with dissipation, such as an attractor (steady point, limit cycle, etc.), bifurcation, or stability of solution, are also suitable for the description of spatial patterns existing far from equilibrium.

Pattern formation in nonlinear dynamical systems have been considered in a wealth of publications. Some 10 –

15 years ago, the mainstream of nonlinear science was represented by investigations of phenomena occurring in point systems, such as complex oscillations, chaos [1 – 4], or stochastic resonance [5]. Today, nonequilibrium patterns in spatially extended dynamical systems constitute the most rapidly developing field in nonlinear physics, chemistry, and biology. Pioneering studies on the propagation of chemical waves in the spatially extended Belousov – Zhabotinsky reaction (BZ reaction) performed in the USSR/Russia [6 – 9] gave impetus to similar research in different countries [10]. The increasingly greater interest in nonequilibrium patterns stems from the experimental discovery of Turing patterns [11], i.e., the patterns predicted by English mathematician Allan Turing in his last work, which appeared in 1952, shortly before his death [12]. An incomplete list of relevant publications for the last 10 years includes scores of reviews and books [13 – 35].

Nonequilibrium patterns are exemplified by elegant dynamical forms (patterns) described by biologists as widespread in the kingdom of microorganisms [36]. Recent discoveries include physiologically important chemical waves of NADPH in living cells (neutrophils protecting humans against the causative agents of many diseases) [37 – 40] and waves of Ca^{2+}, a signal ion that triggers various physiological processes in many cell types. The existence of Ca^{2+} waves has been documented not only inside a cell [41] but also in tissues, e.g., in the brain [42]. Surface waves in liquids, Faraday waves, Taylor rotating fluids [13], Rayleigh – Benard convection cells [43, 44], patterns associated with gas discharges [45 – 47], and granular systems [48] are examples of nonequilibrium patterns in nonlinear physics.

Nonlinear dynamics lays claim to being a universal phenomenon. At present, it fairly well describes patterns extending within a range from a few microns (the size of a living cell) to the planetary scale (ecological systems, climate). However, the very first observations in quantum mechanics [49] and cosmology [50] suggest that laws of nonlinear dynamics are equally applicable in these disciplines, too. This is understandable bearing in mind that these are mathematical laws independent of the nature of forces acting on the system, such as electromagnetic, gravitational, or weak interactions. Dynamical pattern formation in physics, chemistry, biology, environmental science [19], and even the social sciences [51] obeys similar laws. This allows many results obtained in one scientific discipline to be used (with slight modification) in another; that is, patterns found in one dynamical system are likely to be discovered in others.

The universal nature of nonlinear dynamics accounts for the importance of the correct choice of laboratory systems for the study of pattern formation mechanisms. Such systems include a homogeneous chemical reaction discovered by Belousov [52] and interpreted by Zhabotinsky [9]; the $ClO_2 - I^-(I_2) - MA$ reaction (CIMA and CDIMA reactions) [53, 54]; and oxidation of CO on a Pt crystal [55 – 57]. The BZ reaction in water-in-oil microemulsions (BZ – AOT systems) that I have been studying for the last 10 years [58 – 64] turns out to be especially rich in various waves and patterns. Research carried out at Brandeis University resulted in the discovery of new types of waves such as antispirals, wave packets, segmented spirals, and standing and dash waves, as well as oscillatory clusters and oscillatory spots (oscillons).

The present review is focused on nonlinear dynamical patterns in chemical reaction – diffusion systems without convection, which are exemplified by the BZ – AOT system. Accordingly, the corresponding models contain no convective term of the $v\,\partial u/\partial r$ type, where v is the velocity, u is the concentration of the substance, and r is the spatial coordinate.

Two main types of dynamical patterns can be distinguished: waves and stationary patterns. Waves in chemical systems can be classified as trigger or phase. The term 'trigger waves' implies on/off waves in a system switching over from one state to another. The final state of the system through which a wave has passed may coincide with its initial state (double switch). Trigger waves are generated in either oscillatory or stable steady-state media provided the medium is excitable. In most cases, the velocity of trigger waves is given by an expression of the $(D/\tau)^{1/2}$ type, where D is the diffusion coefficient and τ is the characteristic time of autocatalysis.

Phase waves are by definition associated with spatial movements of the phase of oscillations at each point of the space. Therefore, they can exist only in an oscillatory system. Phase waves can have either high or low amplitude and practically any velocity. As regards wave packets (or packet waves), a specific case of phase waves, the amplitude of their oscillations is small and they tend to assume a sinusoid-like form, while their speed is determined by group and phase velocities computed from dispersion curves [63, 65, 66].

Waves can also be classified based on their geometric aspect, in which case they are categorized as plane, concentric, or spiral. Both trigger and phase waves can be spiral or circular with a single center (pacemakers or targets). Depending on the direction of propagation (towards the center or away from it), spiral and phase waves can be classified as 'normal' (i.e., outwardly propagating) and inwardly propagating (antispirals and antipacemakers). To date, only phase waves directed towards the perturbation center are known to exist (in this case, the fundamental principle of causality remains valid).

Packet waves undergoing multiple reflections from walls can transform into standing waves analogous to mechanical standing waves generated by string vibrations and acoustic (or electromagnetic) standing waves. Recently, a periodic excitation of the cardiac muscle from the outside was shown to induce standing waves of excitation classified as a variant of trigger waves [67, 68]. Trigger waves can behave as cars on a motorway having a propensity to create jams or so-called shock structures [69 – 71]. Also well known are solitary waves or solitons [72].

Stationary structures are usually the spatially periodic Turing patterns of a certain wavelength determined by the diffusion coefficient of the reagents and their chemical reactivity [11, 73 – 77]. Also known are structures oscillating in time and having an almost stationary boundary and no definite wavelength. They have been termed clusters [78 – 80]. Clusters are similar to standing waves except that they lack a characteristic wavelength.

The existence of standing waves, oscillatory clusters, and segmented spirals somewhat obscures the disparity between traveling waves and stationary structures. For example, segmented spirals (or dash waves) [64, 81] are actually the propagating 1-D Turing patterns.

Almost all these dynamical patterns have been found in the BZ – AOT system. The main part of this review is preceded by three short sections describing AOT microemulsions (Section 2), the BZ reaction, and the BZ – AOT system (Section 3). The mathematical apparatus for classifying and analyzing different structures (the theory of linear

stability analysis of the homogeneous steady state) is briefly described in Section 4. The bulk of the material is presented in Sections 5–9. Closing Section 10 concerns the prospects of further development of nonlinear dynamics.

2. AOT microemulsions

A water-in-oil AOT microemulsion (ME) can be regarded as a physical milieu in which nanometer-sized water droplets diffuse, collide, fuse, and separate. Some 10 years ago, I chose to work with AOT-ME from a large number of other MEs for the simple reason that it was the ME about which almost everything had been known. This AOT-ME is described in detail in Ref. [82].

A water-in-oil AOT-ME is a thermodynamically stable system composed of three components: water, surfactant (AOT), and oil (a saturated hydrocarbon, e.g., octane used in our experiments). In a BZ–AOT system, reagents of the BZ reaction are dissolved in water, i.e., placed in the aqueous pseudophase (thus called for being a discontinuous aqueous phase). The properties of ME change if a dissolved salt or acid is present in the water at a high concentration (in excess of 0.1 M).

An AOT molecule contains a small polar group (the SO_3^- group) and two long fat tails facing the hydrophobic phase. There is only one way to arrange such molecules close together head to head and tail to tail without intervening gaps. Specifically, their polar heads must look toward the center of the sphere formed by the fat tails (Fig. 1). Such geometric properties of AOT molecules account for the inverse character of AOT-ME in which water cores surrounded by a monolayer of AOT molecules are submerged in the continuous hydrophobic phase (octane).

The radius of the droplet's water core in nanometers is roughly determined as $R_w = 0.17\omega$, where $\omega \equiv [H_2O]/[AOT]$; R_w is independent of the octane volume fraction in ME. The total radius of the droplet together with the surrounding AOT monolayer (hydrodynamic radius) R_d is bigger than R_w by the length of the AOT molecule (around 1.1 nm). The concentration of water droplets can be lowered by simply adding octane to the ME. For this reason, we used to first prepare a concentrated ME and thereafter dilute it to a desired concentration. In the initial concentrated ME, the volume fraction of water ϕ_w is about 0.3 (30%) and that of droplets ϕ_d (together with the surrounding AOT monolayer) amounts to 0.7 (70%). ϕ_d and ϕ_w are roughly related by expression

$$\phi_d \approx \phi_w\left(1 + \frac{21{,}6}{\omega}\right). \quad (1)$$

Many physical properties of an ME show an almost threshold-like dependence on ϕ_d. Such a dependence is due to percolation. If $\phi_d \ll \phi_{cr}$ (with the percolation threshold $\phi_{cr} \cong 0.5$), the ME can be arbitrarily described as a medium in which water droplets float freely. The viscosity of such an ME is almost identical with that of water and the electrical conductivity is similar to that of pure octane. For such an ME, diffusion coefficient D_d of a water droplet and its radius R_d are related by the Stokes–Einstein formula

$$D_d = \frac{kT}{6\pi\eta R_d}, \quad (2)$$

where η is the viscosity of an organic solvent, k is the Boltzmann constant, and T is the temperature. Relation (2) is used to determine the droplet radius in dynamic light scattering experiments. The droplet's diffusion coefficient D_d is one or two orders of magnitude (depending on the droplet radius and ϕ_d) smaller than the diffusion coefficient of low-molecular compounds in octane, approximately 10^{-5} cm^2 s^{-1} [83]. Because all the initial reagents of the BZ reaction are hydrophilic and incorporated in the droplet's water core, their diffusion coefficient is determined by the diffusion coefficient of the entire drop D_d.

Certain intermediate products formed in the course of the BZ reaction, e.g., molecular bromine, Br_2, or radical $BrO_2^\bullet$, are octane-soluble and their diffusion coefficient roughly equals 10^{-5} cm^2 s^{-1}. A significant (10–100-fold) difference between diffusion coefficients of individual intermediates is a key factor responsible for the generation of nonequilibrium structures, such as Turing patterns and antispirals.

Mass exchange between droplets is rather efficient and occurs by the collision–fusion–fission of two droplets. The bimolecular constant of effective collisions between droplets, which lead to their transient merging via small bridges (channels), is on the order of 10^7 M^{-1} s^{-1} [84]. Because the diffusion-controlled constant k_{diff} equals approximately 10^9 M^{-1} s^{-1}, only each hundredth collision results in mass exchange. At a typical droplet concentration in the range of 10^{-5}–10^{-3} M, the characteristic time of mass exchange is estimated at 10^{-4}–10^{-2} s, i.e., a few orders of magnitude smaller than all characteristic times of the BZ reaction (seconds–minutes).

Percolation occurs when the volume fraction of droplets ϕ_d exceeds ϕ_{cr}. From the kinetic standpoint, percolation in AOT-ME can be interpreted as a situation where the rate of droplet fusion exceeds the dimer separation rate. In this case, dynamical water channels are formed that span the entire ME (Fig. 2a). The viscosity and electrical conductivity of such an ME increase by 1–2 and 4–5 orders of magnitude, respectively [83, 85–87]. Schwartz et al. [83] have demonstrated that the diffusion coefficients of water molecules and a hydro-

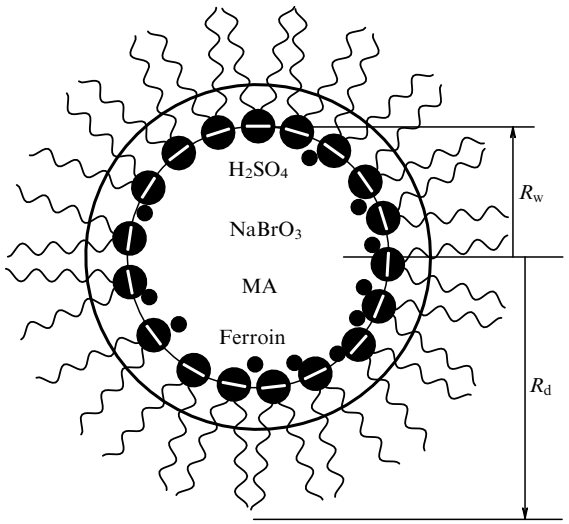

Figure 1. A water droplet of the AOT-microemulsion loaded with the initial reagents of the BZ reaction. R_w — radius of the droplet's water core, R_d — outer radius of the droplet, coincident with the hydrodynamic radius measured experimentally by dynamic light scattering (see Fig. 3).

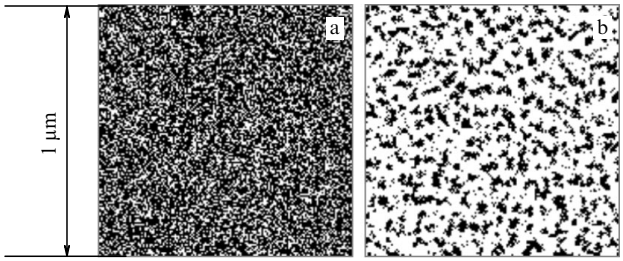

Figure 2. Computer simulation of microemulsion. Each point corresponds to a water droplet: (a) droplet volume fraction $\phi_d = 0.7$ (above the percolation threshold), (b) $\phi_d = 0.3$ (below the percolation threshold).

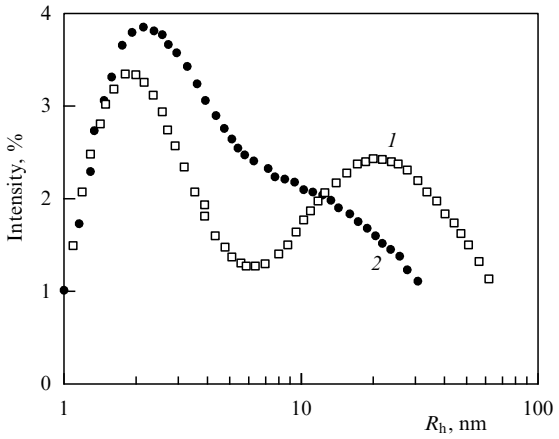

Figure 3. Dependence of relative light scattering intensity on the droplet hydrodynamic radius R_h (droplet distribution by size) obtained in experiments on dynamic light scattering by AOT-microemulsion loaded with the reagents of the BZ reaction ($[H_2SO_4] = 0.4$ M, $[MA] = 0.6$ M): *1* — fresh ME, *2* — the same ME one day later ($\omega = 15$, $\phi_d = 0.55$).

carbon in such an ME are practically identical ($\cong 10^{-5}$ cm^2 s^{-1}).

In the narrow range of droplet concentrations where $\phi_d \cong \phi_{cr}$, clusters are formed (Fig. 2b). Used in this context, the term 'cluster' has the traditional meaning of a set of individual elements as opposed to the term 'oscillatory cluster' in which 'cluster' implies the identity of phases and amplitudes of concentration oscillations in a certain spatial region.

In a three-component system, the droplet distribution by size is rather narrow even if clusters are formed. Hence, AOT-ME may be referred to as a monodispersed system. However, we observed the bimodal droplet distribution by size at a high salt concentration in the aqueous pseudophase (Fig. 3); it very slowly (over a few days) relaxed to the monomodal distribution with the expected droplet radius $R_d = (0.17\omega + 1.1)$ nm. The behavior of AOT-ME containing salts and strong acids at high concentrations needs to be studied in more detail.

3. Belousov – Zhabotinsky reaction and its models

The BZ reaction has been thoroughly investigated (see, e.g., a review by Taylor [28]). The reaction is essentially oxidation of malonic acid (MA) by bromate in an acidic aqueous solution. Initially, Belousov (see his paper in Ref. [10]) used citric acid instead of MA. A large number of other organic substrates can also be used for this purpose. In particular, cyclohexanedione is a popular compound [88], with which no CO_2 bubbles are formed. The BZ reaction is catalyzed by metallic ions and metallocomplexes such as Ce^{3+}, Mn^{2+}, $Fe^{2+}(phen)_3$, and $Ru^{2+}(bpy)_3$, where phen stands for phenanthroline and bpy is bipyridine [10]. The last two metallocomplexes are most often used to observe waves and patterns because they are easy to watch with optical instruments.

The chemical mechanism underlying the BZ reaction may involve three dozen elementary reactions [10, 89, 90]. Working with it is virtually impossible, especially in the analysis of spatial patterns. Fortunately, there are simpler models on which major characteristics of the BZ reaction can be studied.

One such model resembling the well-known FKN mechanism [91] includes six variables and twelve reactions,

$$\mathrm{Y} \to \mathrm{X} + \mathrm{P}\,, \qquad k_1\,, \tag{3}$$

$$\mathrm{X} + \mathrm{Y} \to 2\mathrm{P}\,, \qquad k_2\,, \tag{4}$$

$$\mathrm{X} \to 2\mathrm{X} + 2\mathrm{Z}\,, \qquad k_3\,, \tag{5}$$

$$2\mathrm{X} \to \mathrm{P}\,, \qquad k_4\,, \tag{6}$$

$$\mathrm{Y} + \mathrm{P} \to \mathrm{W}\,, \qquad k_\mathrm{Y}\,, \tag{7}$$

$$\mathrm{W} \to \mathrm{Y} + \mathrm{P}\,, \qquad k_\mathrm{H}\,, \tag{8}$$

$$\mathrm{W} + \mathrm{MA} \to \mathrm{Y}\,, \qquad k_\mathrm{W}\,, \tag{9}$$

$$\mathrm{P} + \mathrm{MA} \to \mathrm{BrMA}\,, \qquad k_\mathrm{P}\,, \tag{10}$$

$$\mathrm{Z} + \mathrm{BrMA} \to \mathrm{Y}\,, \qquad k_\mathrm{Z}\,, \tag{11}$$

$$\mathrm{Z} + \mathrm{MA} \to 0\,, \qquad k_\mathrm{M}\,, \tag{12}$$

$$\mathrm{W} \to \mathrm{U}\,, \qquad k_\mathrm{F}\,, \tag{13}$$

$$\mathrm{U} \to \mathrm{W}\,, \qquad k_\mathrm{B}\,, \tag{14}$$

where $X = HBrO_2$, $Y = Br^-$, Z = ferriin (oxidized form of ferroin), P = HOBr, $W = Br_2$ in the aqueous phase, and $U = Br_2$ in octane. Concentrations of the MA and bromomalonic acid (BrMA) are assumed to be constant. The X molecule is an activator because it autocatalitically reproduces itself in reaction (5). The particle Y is an inhibitor killing the activator and suppressing autocatalysis in reaction (4). Its critical concentration y_{cr} is found from the equality of reaction (4) and (5) rates as $y_{cr} = k_3/k_2$. The autocatalysis is inhibited at $y > y_{cr}$. In the course of the autocatalytic reaction, the catalyst (cat) is transformed into an oxidized state denoted by Z [e.g., $Fe^{3+}(phen)_3$]. An organic substrate, malonic acid, is used to reduce the catalyst. Part of malonic acid is brominated in the BZ reaction and the resulting bromomalonic acid also interacts with the oxidized state of the catalyst. This interaction results in the release of the inhibitor Y. Chemical negative feedback is thus realized. The combination of positive (autocatalysis) and negative feedback mechanisms in the BZ reaction gives rise to oscillations in a well-mixed (often, flow-through) reactor. The described mechanism is fairly precise but remains complicated.

It is necessary to simplify scheme (3) – (14) in order to be able to describe the BZ reaction by a small number of differential equations. This goal is attained by the application of the Oregonator model [92], which perfectly fits the homogeneous BZ reaction.

But the Oregonator model is insufficient for the BZ – AOT system because it fails to describe the rapid diffusion of

Br_2 and $BrO_2^{\bullet}$ molecules in the organic phase. Therefore, I have modified the Oregonator model as follows:

$$\mathrm{Y} \to \mathrm{X}\,, \qquad k_1\,, \tag{15}$$

$$\mathrm{Y} + \mathrm{X} \to 0\,, \qquad k_2\,, \tag{16}$$

$$\mathrm{X} \to 2\mathrm{X} + 2\mathrm{Z}\,, \qquad k_3\,, \tag{17}$$

$$2\mathrm{X} \to 0\,, \qquad k_4\,, \tag{18}$$

$$\mathrm{Z} \to h\mathrm{Y}\,, \qquad k_5\,, \tag{19}$$

$$\mathrm{X} \to \mathrm{S}\,, \qquad k_6\,, \tag{20}$$

$$\mathrm{S} \to \mathrm{X}\,, \qquad k_7\,, \tag{21}$$

$$\mathrm{Z} \to \mathrm{V}\,, \qquad k_8\,, \tag{22}$$

$$\mathrm{V} \to \mathrm{U}\,, \qquad k_9\,, \tag{23}$$

$$\mathrm{U} \to \mathrm{V}\,, \qquad k_{10}\,, \tag{24}$$

$$\mathrm{V} \to \mathrm{Z}\,, \qquad k_{11}\,, \tag{25}$$

$$\mathrm{U} \to \mathrm{S}\,, \qquad k_{12}\,, \tag{26}$$

where S is Br_2O_4 or $BrO_2^{\bullet}$ (second activator) in the organic phase, V is Br_2 in the surfactant pseudophase (inside a surfactant shell of water nanodroplets), U is Br_2 in the organic phase (as before), and h is the stoichiometric coefficient. Reactions (15)–(19) correspond to the original Oregonator model [92]. Reactions (20) and (21) describe the mass exchange by activator particles between the disperse phase (water droplets) and the organic phase; reactions (22)–(25) describe the mass exchange by inhibitor particles among three phases (with the surfactant phase occurring because the solubility of Br_2 in the AOT surfactant is six times its solubility in octane [93]). Reactions (22) and (25) may look strange because the oxidized form of the catalyst (Z) cannot turn into Br_2 (V). However, these reactions are no more strange than reaction (19) in which Z transforms into Br^- (Y). Both Z and V are chemically related through reactions (19) [or (11)], (7), and (13). The particles Z and U (Br_2) serve as inhibitors: Z plays this role in the reduced Oregonator equations with two variables [94] (with the true inhibitor Y excluded), and Br_2 in model (3)–(14) because Br_2 yields bromide (Y) in reaction (8). It is important that Z and U have significantly different diffusion coefficients; they are therefore considered to act as two different inhibitors in reactions (22)–(25). Reaction (26) is an ancillary one (of minor importance) and can be chemically interpreted as $Br_2 \to Br^- \to Br^{\bullet} \to BrO_2^{\bullet}$.

The original ODEs for reactions (15)–(26) have the form

$$\frac{\mathrm{d}[x]}{\mathrm{d}t} = k_1[y] - k_2[x][y] + k_3[x] - k_4[x]^2 - k_6[x] + k_7[s]\,, \tag{27}$$

$$\frac{\mathrm{d}[y]}{\mathrm{d}t} = -k_1[y] - k_2[x][y] + k_5 h[z]\,, \tag{28}$$

$$\frac{\mathrm{d}[z]}{\mathrm{d}t} = 2k_3[x] - k_5[z] - k_8[z] + k_{11}[v]\,, \tag{29}$$

$$\frac{\mathrm{d}[s]}{\mathrm{d}t} = k_6[x] - k_7[s] + k_{12}[u]\,, \tag{30}$$

$$\frac{\mathrm{d}[u]}{\mathrm{d}t} = k_9[v] - k_{10}[u] - k_{12}[u]\,, \tag{31}$$

$$\frac{\mathrm{d}[v]}{\mathrm{d}t} = k_8[z] - k_9[v] + k_{10}[u] - k_{11}[v]\,. \tag{32}$$

By introducing the dimensionless variables

$$[x] = \frac{k_3 x}{2k_4}\,, \quad [y] = \frac{k_3 y}{k_2}\,, \quad [z] = \frac{k_3^2 z}{k_4 k_5}\,,$$

$$t = \frac{\tau}{k_5}\,, \quad [s] = \frac{k_3^2 s}{2k_4 k_7}\,, \quad [v] = \frac{k_3^2 v}{k_4 k_{11}}\,, \quad [u] = \frac{k_3^2 u}{2k_4 k_{10}}$$

and the new parameters

$$f = 2h\,, \quad q = \frac{2k_4 k_1}{k_3 k_2}\,, \quad \varepsilon = \frac{k_5}{k_3}\,, \quad \beta = \frac{k_6}{k_3}\,,$$

$$\alpha' = \frac{k_8}{k_5}\,, \quad K = \frac{k_9}{k_{11}}\,, \quad \alpha = \frac{\alpha' K}{1+K}\,, \quad \gamma = \frac{1}{2(1+K)}\,,$$

$$\varepsilon_2 = \frac{k_5}{k_6}\,, \quad \varepsilon_3 = \frac{k_5}{2k_{10}} \ll 1\,, \quad \varepsilon_4 = \frac{k_5}{k_{11}} \ll 1\,,$$

$$\varepsilon' = \frac{2k_4 k_5}{k_3 k_2} \ll 1\,, \quad \chi = \frac{k_{12}}{k_{10}}\,,$$

we transform Eqns (27)–(32) to the dimensionless form

$$\varepsilon \frac{\mathrm{d}x}{\mathrm{d}\tau} = qy - yx + x - x^2 - \beta x + s\,, \tag{33}$$

$$\varepsilon' \frac{\mathrm{d}y}{\mathrm{d}\tau} = -qy - yx + fz = 0\,, \tag{34}$$

$$\frac{\mathrm{d}z}{\mathrm{d}\tau} = x - z - \alpha' z + v\,, \tag{35}$$

$$\varepsilon_2 \frac{\mathrm{d}s}{\mathrm{d}\tau} = \beta x - s + \chi u\,, \tag{36}$$

$$\varepsilon_3 \frac{\mathrm{d}u}{\mathrm{d}\tau} = Kv - \frac{u}{2} - \frac{\chi u}{2}\,, \tag{37}$$

$$\varepsilon_4 \frac{\mathrm{d}v}{\mathrm{d}\tau} = \alpha' z - Kv + \frac{u}{2} - v = 0\,. \tag{38}$$

Because $\varepsilon' \ll 1$ and $\varepsilon_4 \ll 1$, the variables y and v can be eliminated via quasi-equilibrium conditions, $y = fz/(q+x)$ and $v = (\alpha' z + u/2)/(1+K)$.[1] The final model with four variables and added diffusion terms has the form

$$\frac{\partial x}{\partial \tau} = \frac{1}{\varepsilon}\left(\frac{fz(q-x)}{q+x} + x - x^2 - \beta x + s\right) + \frac{D_x}{D_u}\,\Delta x\,, \tag{39}$$

$$\frac{\partial z}{\partial \tau} = x - z - \alpha z + \gamma u + \frac{D_z}{D_u}\,\Delta z\,, \tag{40}$$

$$\frac{\partial s}{\partial \tau} = \frac{1}{\varepsilon_2}(\beta x - s + \chi u) + \frac{D_s}{D_u}\,\Delta s\,, \tag{41}$$

$$\frac{\partial u}{\partial \tau} = \frac{1}{\varepsilon_3}\left[\alpha z - \left(\gamma + \frac{\chi}{2}\right)u\right] + \frac{D_u}{D_u}\,\Delta u\,, \tag{42'}$$

where the Laplacian is $\Delta \equiv \partial^2/\partial r^2$ in the 1-D case and $\Delta \equiv \partial^2/\partial x^2 + \partial^2/\partial y^2$ in the 2-D case (where x and y are the spatial coordinates). Because $\chi \ll \gamma$, Eqn (42′) can be simplified by assuming $\chi = 0$:

$$\frac{\partial u}{\partial \tau} = \frac{1}{\varepsilon_3}(\alpha z - \gamma u) + \Delta u\,. \tag{42}$$

The diffusion coefficients D_x and D_z are equal to the diffusion coefficient of the entire nanodroplet of water (approximately

[1] This procedure is not innocuous and can change the Andronov–Hopf bifurcation type from subcritical to supercritical in a wide range of system parameters.

10^{-7} cm^2 s^{-1} [83]), whereas the coefficients D_s and D_u are roughly equal to the diffusion coefficient of low molecular weight molecules in octane (of the order of 10^{-5} cm^2 s^{-1}).

In the dimensionless model (39)–(42), dimensionless diffusion coefficients of a D_x/D_u type are used. To facilitate the transition from the dimensionless unit length to the dimensional one (for quantitative comparison of experimental and simulated patterns), the former should by multiplied by $(D_u/k_5)^{1/2}$. For example, if $D_u = 10^{-5}$ cm^2 s^{-1} and $k_5 = 0.1$ s^{-1}, then the dimensionless unit is 0.1 mm. Model (39)–(42) allows us to describe practically all wave instabilities and the Turing instability phenomena found in the BZ–AOT system.

It is worthwhile to note that model (39)–(42) simulates a homogeneous system that does not explicitly contain such parameters as the droplet size R_d and the volume fraction ϕ_d of a microheterogeneous AOT-microemulsion. Because the size of water nanodroplets is four orders of magnitude smaller than all characteristic sizes of the observed waves and nonequilibrium patterns, I believe it is justified to describe this medium as homogeneous with the help of the standard reaction–diffusion equations (the term 'standard' means that all nondiagonal elements of the matrix of diffusion coefficients are zero). The parameters R_d and ϕ_d of the microemulsion are implicitly involved in the diffusion coefficients and in the constants of mass exchange between phases (α, β, γ). The case of nonzero nondiagonal terms in the matrix of diffusion coefficients (cross diffusion) and the case where fluctuations must be taken into account (fluctuations of concentrations and rate constants in nanodroplets are significant) are beyond the scope of the present review.

4. Linear stability analysis

The linear stability analysis of the steady state of a reaction–diffusion system of type (39)–(42) reveals two main types of diffusive instability: the Turing instability and the wave instability [34]. In the case of the Turing instability, the real part of the eigenvalue of the characteristic equation, $\mathrm{Re}\,\Lambda$, is positive for a certain finite interval of wave numbers $\mathbf{k} > 0$ and has a maximum at a certain $\mathbf{k} = \mathbf{k}_T$, while, as a rule, $\mathrm{Re}\,\Lambda < 0$ at $\mathbf{k} = 0$ and the imaginary part $\mathrm{Im}\,\Lambda$ is equal to zero. In this situation, concentration patterns periodic in space and stationary in time are formed; they are referred to as the Turing patterns. In the case of wave instability, $\mathrm{Re}\,\Lambda$ is also positive in a certain range of wave numbers, but the imaginary part is nonvanishing. This gives rise to waves and patterns periodic in both time and space. Turing described both types of instability in his classic work [12].

Techniques for linearization of reaction–diffusion equations (evaluation of the Jacobian) and determination of the eigenvalues Λ of characteristic equations are fairly well described in the literature [95]. Any infinitesimally small deviation of the system from its equilibrium changes with time as $\exp(\Lambda t + \mathrm{i}\mathbf{kr})$. Therefore, the system continues to deviate farther and farther from the equilibrium if $\mathrm{Re}\,\Lambda > 0$ at a certain $\mathbf{k}$. In such a case, it is called unstable. For model (39)–(42), the characteristic determinant is written as

$$\begin{vmatrix} A_{11} - \mathbf{k}^2 D_x - \Lambda & A_{12} & A_{13} & A_{14} \\ A_{21} & A_{22} - \mathbf{k}^2 D_z - \Lambda & A_{23} & A_{24} \\ A_{31} & A_{32} & A_{33} - \mathbf{k}^2 D_s - \Lambda & A_{34} \\ A_{41} & A_{42} & A_{43} & A_{44} - \mathbf{k}^2 D_u - \Lambda \end{vmatrix}, \tag{43}$$

where the diffusion coefficients D_x, D_z, D_s, and D_u are dimensionless quantities,

$$A_{11} = \frac{1}{\varepsilon}\left[1 - 2x_{SS} - \beta - \frac{2qfz_{SS}}{(x_{SS}+q)^2}\right],$$

$$A_{12} = \frac{1}{\varepsilon}\frac{f(q - x_{SS})}{x_{SS}+q}, \qquad A_{13} = \frac{1}{\varepsilon},$$

$$A_{14} = A_{23} = A_{32} = A_{41} = A_{43} = 0,$$

$$A_{21} = 1, \qquad A_{22} = -1 - \alpha, \qquad A_{24} = \gamma,$$

$$A_{31} = \frac{\beta}{\varepsilon_2}, \qquad A_{33} = -\frac{1}{\varepsilon_2}, \qquad A_{34} = \frac{\chi}{\varepsilon_2},$$

$$A_{42} = \frac{\alpha}{\varepsilon_3}, \qquad A_{44} = \frac{\gamma}{\varepsilon_3},$$

and the steady-state value x_{SS} is found from the solution of the quadratic equation

$$x_{SS} = 0.5\left\{B + \left[B^2 + 4q\left(1 + \frac{\chi\alpha}{\gamma} + f\right)\right]^{1/2}\right\}, \tag{44}$$

where $B = 1 + \chi\alpha/\gamma - q - f$ and $z_{SS} = x_{SS}$. Although the analytic solution of the 4th-order equation is known, we use it only to facilitate the numerical evaluation of dispersion curves, i.e., plots of $\mathrm{Re}\,\Lambda$ and $\mathrm{Im}\,\Lambda$ versus the wave number $\mathbf{k}$. A complete analysis of determinant (43) has never been made nor have the regions in the parameter space where wave and Turing instabilities occur been found.

Typical dispersion curves for model (39)–(42) are presented in Fig. 4. In the case of both wave and Turing instabilities, the diffusion coefficients of the activator D_{act} and the inhibitor D_{inh} are identical regardless of whether they diffuse slowly or rapidly. For the model with two variables, there is a theorem stating that a homogeneous steady state can lose its stability via Turing instability only when $D_{inh} > D_{act}$ [32]. Incidentally, this theorem does not exclude the existence of a Turing pattern at $D_{inh} = D_{act}$ unless the initial state is homogeneous [96]. It can be seen from the caption in Fig. 4 that there is no such limitation for the model with four variables, even though a rapidly and slowly diffusing activator and inhibitor must be present. Turing patterns cannot arise in the absence of a rapidly diffusing inhibitor.

The dispersion curves in Fig. 4 suggest that it is possible to obtain all types of instabilities, including the Andronov–Hopf instability characterized by positive $\mathrm{Re}\,\Lambda$ at $\mathbf{k} = 0$, by means of a small variation in the diffusion coefficients or the parameters of mass exchange between the aqueous and oil phases. It is worthy of note that the dispersion curves with negative dispersion ($\mathrm{d}\,\mathrm{Im}\,\Lambda/\mathrm{d}k < 0$ at $\mathbf{k} = \mathbf{k}_w$) presented in Fig. 4b offer a plausible explanation for the new type of spiral waves, antispirals, discovered by us and described in Refs [62, 63].

Because a 4th-order equation may have two complex roots, the case of two wave instabilities (when real parts of two complex eigenvalues have positive maxima at different wave numbers) is equally feasible and was theoretically predicted. To date, however, no experimental data are available that require such a complicated case to be used for their explanation.

5. Turing patterns

Turing patterns were discovered by Patrick De Kepper's group in 1990 [11, 73], i.e., 38 years after they had been

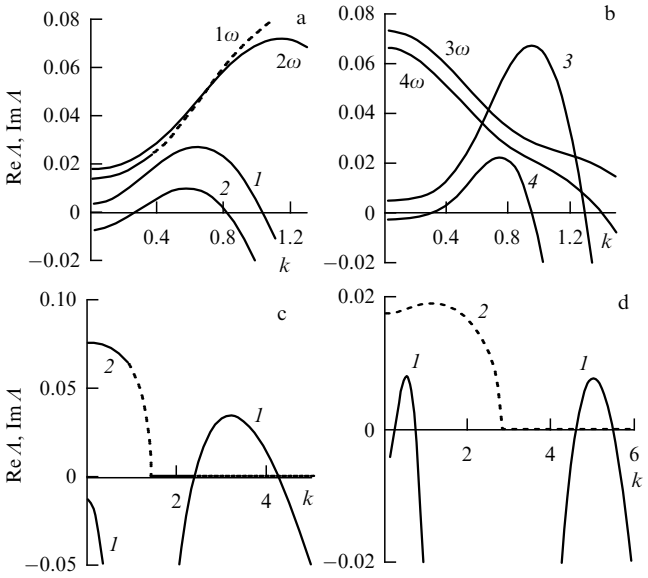

Figure 4. Dispersion curves of model (39)–(42): (a) wave instability with positive dispersion, $\mathrm{d}\,\mathrm{Im}\,\Lambda/\mathrm{d}k > 0$; (b) wave instability with negative dispersion, $\mathrm{d}\,\mathrm{Im}\,\Lambda/\mathrm{d}k < 0$; (c) Turing instability; (d) concurrent Turing and wave instabilities. Curves *1–4* in Figs a and b, curves *1* in Figs c and d — $\mathrm{Re}\,\Lambda$. Curves $1\omega-4\omega$ in Figs a and b are the corresponding imaginary parts displaced downward by 0.97, 0.92. 1.245, and 1.17, respectively. Curves *2* in Figs (c, d) are $\mathrm{Im}\,\Lambda/10$. The parameters of model (39)–(42): (a) $q = 0.0015$, $f = 1.4$, $\varepsilon = 0.34$ (curve *1*), $\varepsilon = 0.36$ (curve *2*), $\varepsilon_2 = 1.4$, $\varepsilon_3 = 0.006$, $\alpha = 6$ (curve *1*), $\alpha = 7$ (curve *2*), $\beta = 0.32$, $\gamma = 0.2$, $\chi = 0$, $D_x = D_z = 0.01$, $D_s = D_u = 1$; (b) $q = 0.0033$, $f = 1.5$, $\varepsilon = 0.4$ (curve *3*), $\varepsilon = 0.385$ (curve *4*), $\varepsilon_2 = 3.5$ (curve *3*), $\varepsilon_2 = 3.2$ (curve *4*), $\varepsilon_3 = 0.0016$ (curve *3*), $\varepsilon_3 = 0.0024$ (curve *4*), $\alpha = 6.2$ (curve *3*), $\alpha = 6.3$ (curve *4*), $\beta = 0.28$ (curve *3*), $\beta = 0.275$ (curve *4*), $\gamma = 0.1$, $\chi = 0.00595$ (curve *3*), $\chi = 0.004$ (curve *4*), $D_x = D_z = 0.01$ (curve *3*), $D_x = D_z = 0.015$ (curve *4*), $D_s = D_u = 0.9$ (curve *3*), $D_s = D_u = 1$ (curve *4*); (c) $q = 0.002$, $f = 1.9$, $\varepsilon = 0.5, \alpha = 12, \beta = 0.1, \gamma = 0.1, \varepsilon_2 = 1, \varepsilon_3 = 0.01, \chi = 0, D_x = D_z = 0.01$, $D_s = D_u = 1$; (d) $q = 0.0015$, $f = 1.4$, $\varepsilon = 0.37$, $\alpha = 9$, $\beta = 0.34$, $\gamma = 0.2$, $\varepsilon_2 = 1.3$, $\varepsilon_3 = 0.006$, $\chi = 0$, $D_x = D_z = 0.01$, $D_s = 1$, $D_u = 0.85$.

predicted theoretically. They were found in a homogeneous chemical system containing chlorite, iodide, and malonic acid at the temperature +5 °C. The discovery was followed by the works of two groups, one headed by Epstein and the other by Swinney [74–76], which explicitly demonstrated various types of Turing patterns and offered their theoretical explanation (the model then proposed has been successfully employed up to now). All these studies gave impetus to theoretical research, e.g., classifying Turing patterns in terms of symmetry, and discussion of the role of these structures in morphogenesis. The latest experimental results on Turing patterns in the CIMA–CDIMA system concern spatially periodic effects on these structures and modes of their spatial propagation at various initial perturbations, including splitting individual spots [97–103].

The BZ–AOT system is the second experimental chemical system in which Turing patterns can be found, in this case, at room temperature (23 °C) and under very simple experimental conditions using no special reactor to continuously supply a thin reactive layer with new reagents. Our 'reactor' consists of two flat optical glasses separated by a thin (80–100 μm) Teflon gasket with an inner diameter of 25 mm and an outer diameter of 50 mm. The inside of the reactor, 25 mm in diameter, is filled with an AOT microemulsion leaving no free space for air bubbles. The two glasses are slightly pressed

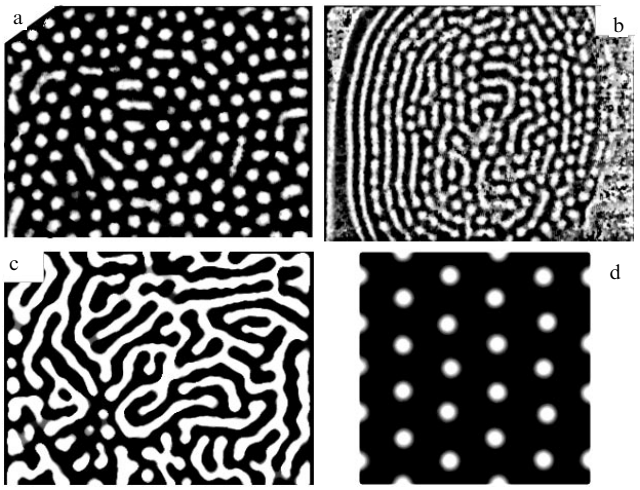

Figure 5. Turing patterns in the BZ–AOT system (a–c) and in model (3)–(14) (d). $[H_2SO_4]_0 = 0.2$ M; $[NaBrO_3]_0 = 0.2$ M (Fig. a), 0.18 M (Fig. b), 0.17 M (Fig. c); $[MA]_0 = 0.3$ M; $[\text{ferroin}]_0 = 4$ mM, $\omega = 15$; $\phi_d = 0.36$ (Fig. a), 0.35 (Fig. b, c). Snapshot size: (a, c) 2.6×1.9 mm, (b) 3.8×2.8 mm, (d) 50×50 [dimensionless units to be multiplied by $(10^{-5})^{1/2}$ to pass to centimeters]. Black and white colors correspond to elevated ferrion and ferriin (z) concentrations, respectively. Parameters of model (3)–(14): $k_1 = 0.05\ \mathrm{s}^{-1}$, $k_2 = 10^6\ \mathrm{M}^{-1}\ \mathrm{s}^{-1}$, $k_3 = 0.25\ \mathrm{s}^{-1}$, $k_4 = 1000\ \mathrm{M}^{-1}\ \mathrm{s}^{-1}$, $k_V = 10^7\ \mathrm{M}^{-1}\ \mathrm{s}^{-1}$, $k_H = 50\ \mathrm{s}^{-1}$, $k_W = 2\ \mathrm{M}^{-1}\ \mathrm{s}^{-1}$, $k_P = 0.2\ \mathrm{M}^{-1}\ \mathrm{s}^{-1}$, $k_Z = 0.3\ \mathrm{M}^{-1}\ \mathrm{s}^{-1}$, $k_M = 0.15\ \mathrm{M}^{-1}\ \mathrm{s}^{-1}$, $k_F = 2000\ \mathrm{s}^{-1}$, $k_B = 200\ \mathrm{s}^{-1}$, $D_x = D_y = D_z = D_p = D_w = 0.05$, $D_u = 1$.

together. Patterns are observed through a stereomicroscope equipped with a digital charge-coupled device (CCD) camera connected to a computer. The reactor is illuminated through an interference filter with the wavelength at which the catalyst has its absorption maximum. This wavelength is 508 nm for ferroin, 450 nm for the $Ru(bpy)_3^{2+}$ complex, and 532 nm for the bathoferroin.

Typical Turing patterns stationary in time are shown in Fig. 5a–c. They have the form of spots (a), spots with stripes (b), and a labyrinth (c). In all these cases, the typical spatial wavelength of the Turing structures is roughly 0.2 mm. For these structures to be seen, the volume fraction of nanodroplets must be smaller than the percolation threshold ($\phi_d < 0.5$) and the point BZ–AOT system (the same system in a well-mixed reactor) must be close to the steady-state–oscillations borderline (i.e., to the onset of the Andronov–Hopf bifurcation). Figure 5b shows patterns that emerge from the incoming trigger waves. As the latter come close to the zone with Turing patterns, they first stand still, giving rise to stripe-like structures, which then slowly (within minutes or dozens of minutes) begin to develop breaks and eventually transform into spots. Because the experiment is conducted in a closed reactor supplied with no fresh reactants, the lifetime of our structures is limited (a few hours), and they gradually disappear.

For comparison, Fig. 5d shows Turing patterns obtained in model (3)–(14) where only Br_2 in octane can rapidly diffuse. In many cases, experimental structures are not regular hexagonal spots as in the models. I believe that the process of spot adjustment (or restructuring) to a regular geometric shape takes much time, which a closed system lacks. However, selected experiments yielded ideally shaped hexagonal Turing patterns. Similar hexagonal spots were obtained in model (39)–(42) with the parameters shown in Fig. 4c. In all models of the BZ–AOT system, a rapidly

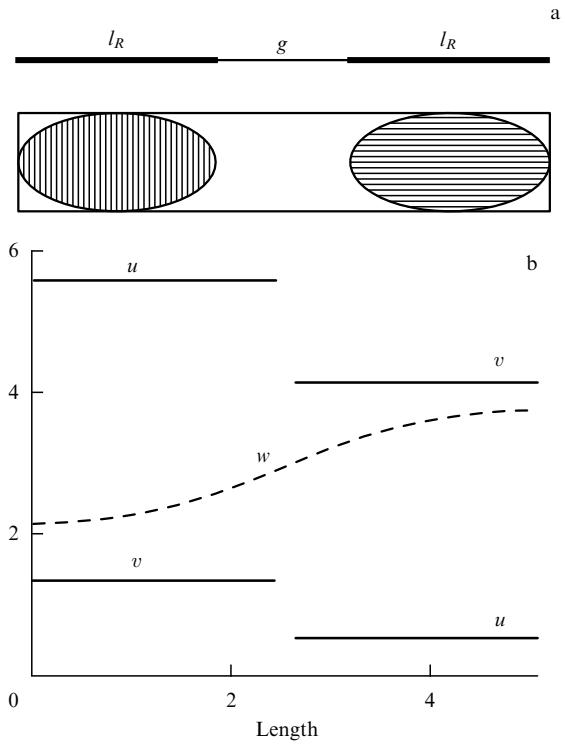

Figure 6. (a) Heterogeneous system of two identical water droplets (two microreactors) of size l_R with a gap g between them. (b) Turing pattern for heterogeneous system (45)–(47), $l_R/g = 0.01$, $l_R/\lambda_T = 0.165$; $\lambda_T = 14.91$ ($\lambda_T = 2\pi/k_{min}$, where k_{min} is the smallest wave number when $\mathrm{Re}\,\Lambda = 0$); $L = 2l_R + g = 5.0856$. $D_u = D_v = D_w = 100$ in droplets and $D_u = D_v = 0$, $D_w = 100$ in the gap; $a = 3.06$, $b = 7$, $d = 5$, $c = 2$, curve w — $10(w - 0.8)$.

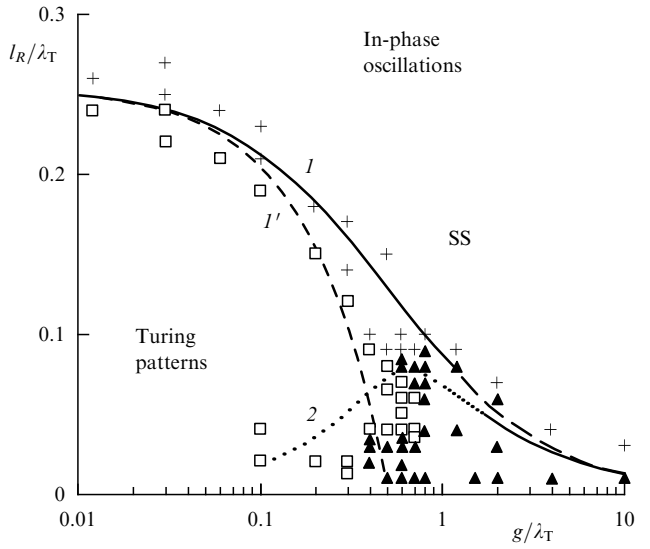

Figure 7. Parametric diagram obtained by numerical computation of heterogeneous system (45)–(47). Parameters: $a = 3.06$, $b = 7$, $c = 2$, $d = 5$. Curve *1′* corresponds to $(2l_R + g)/\lambda_T = 0.5$; $\lambda_T = 14.91$, curve *1* to $(2l_R + g')/\lambda_T = p$, $p = 0.5$, $g' = p\lambda_T g/(p\lambda_T + g)$, curve *2* $k_1 = \mathbf{k}^2 D_w = k_{1\text{-cr}}$ [110] outlines the area of theoretical in-phase oscillations. □ — Turing patterns, + — steady state (SS), ▲ — in-phase oscillations.

diffusing inhibitor (Br_2 or Z) is indispensable for the realization of Turing patterns.

Today, three basic types of Turing patterns are known, viz. hexagonal spots, stripes, and honeycomb-like structures that can be regarded as inverted hexagonal spots. These patterns have been found in an experiment using a chlorite-iodide system [76] and in computer simulations [104]. Turing structures of a more complex shape have recently been reported to which beautiful names such as 'black eye', 'white eye', etc. were given by the authors [99, 105, 106]. They are formed by virtue of interactions between the simplest forms of Turing patterns (with different wavelengths) realized in neighboring thin layers [103, 107]. It may be inferred from purely theoretical considerations that, the labyrinth-like patterns in Fig. 5c being stable, Turing structures must have an infinitely large number of forms. This situation is analogous to obtaining regular oscillations with any predetermined period from chaotic oscillations for a 0-D system [108].

So far, only Turing patterns in a homogeneous environment have been considered, and theoretical discussions on the role of these structures in morphogenesis have ignored the simple fact that dividing cells make a heterogeneous medium. The idea of a rapidly diffusing second inhibitor (Br_2) regarded as a messenger between water droplets is readily applicable to a real heterogeneous medium with large drops (analogs of living cells) commensurable with the characteristic size of Turing patterns and separated by a gap (analog of the intercellular space) through which only this messenger (signal molecule) can diffuse.

We now consider the system in Fig. 6a. Let a pair of identical water droplets be filled with a dynamical system having positive (autocatalysis) and negative (inhibition) feedback. For simplicity, we choose the well-known Brusselator model [109] [Eqns (45) and (46) at $c = d = 0$], extended by introducing a rapidly diffusing second inhibitor (w):

$$\frac{\partial u}{\partial t} = a - (1 + b)u + u^2 v + D_u \frac{\partial^2 u}{\partial x^2}\,, \tag{45}$$

$$\frac{\partial v}{\partial t} = bu - u^2 v - cv + dw + D_v \frac{\partial^2 v}{\partial x^2}\,, \tag{46}$$

$$\frac{\partial w}{\partial t} = cv - dw + D_w \frac{\partial^2 w}{\partial x^2}\,. \tag{47}$$

The main inhibitor (v) is linearly related to the second (w), which is able to diffuse both within the droplets and through the gap (messenger). In contrast, the activator (u) and inhibitor molecules are confined to the inside of the droplets. The equalities $D_u = D_v = a = b = c = d = u = v = 0$ are fulfilled in the gap and the equalities $D_u = D_v = D_w$ in the droplets. In addition, we choose the parameters a, b, c, and d such that system (45)–(47) remains in a stable steady state (with stationary values of $u_{SS} = a$, $v_{SS} = b/a$, and $w_{SS} = cb/ad$).

If the gap between the droplets is not too large, the homogeneous steady state of heterogeneous system (45)–(47) (having the geometry shown in Fig. 6) may lose stability. In this case, the two droplets pass to new (and different) steady states analogous to the maximum and minimum in the Turing structures (Fig. 6b) [110]. This type of symmetry breaking is more suitable for speculation on diffusive instabilities in the course of morphogenesis. Figure 7 illustrates dependences of two identical droplets on their own size and the size of the gap. Evidently, a stable homogeneous steady state (SS) and Turing patterns (in the sense of the structure shown in Fig. 6b) exist concurrently with synchronous relaxation oscillations, whose amplitude is

bigger than that of the Turing patterns and the period is strongly dependent on the gap size [110]. The appearance of in-phase oscillations in a system of two coupled identical dynamical subsystems in a steady state is due to a delay in signal transmission between these subsystems (droplets) [111–114]. The bigger the gap, the longer the delay. The oscillations occur only within a certain range of mean time delays.

6. Wave instability

The wave instability in reaction–diffusion systems is still poorly known. The first theoretical works (apart from the classical work of Turing [12]) date to the 1980s–1990s [66, 95]. The first experiments were carried out quite recently [61, 63, 115]. Comparison of the properties of wave packets (and standing waves) in chemical systems and in physics (optics, acoustics, physics of surface, and hydrodynamic waves) reveals many similarities as well as certain differences. We propose the term 'chemical optics' to define a group of phenomena related to wave properties of reaction–diffusion systems.

For a wave instability (characterized by the dispersion curves shown in Fig. 4 a, b) to occur, a chemical system must have at least three variables. This inference readily ensues from the analysis of the quadratic characteristic equation for a system with two variables,

$$2\Lambda_{1,2} = \mathrm{Tr}\, A \pm \left[\mathrm{Tr}\,(A)^2 - 4\det A\right]^{1/2}, \qquad (48)$$

where $\mathrm{Tr}\, A$ is the trace of the characteristic matrix A [of type (43)] and $\det A$ is its determinant. For the wave instability, $\mathrm{Re}\,\Lambda = \mathrm{Tr}\, A$, $\mathrm{Im}\,\Lambda \neq 0$, and the trace $\mathrm{Tr}\, A$ must be a nonmonotonic function of the wave number $\mathbf{k}$. However, for a system with two variables,

$$\mathrm{Tr}\, A = a_{11} + a_{22} - \mathbf{k}^2(D_\mathrm{u} + D_\mathrm{v})\,.$$

In other words, $\mathrm{Tr}\, A$ is a monotonic function of $\mathbf{k}$; hence, it can have no maximum at $k > 0$ necessary for the wave instability to occur.

Our numerous computer simulations have demonstrated that any reaction–diffusion system with two variables of the activator–inhibitor type can develop a wave instability after the addition of the third variable, i.e., the second rapidly diffusing activator linearly related to the 'main' slowly diffusing activator. In the BZ–AOT system, the role of the slowly diffusing activator is played by $HBrO_2$ molecules present in water droplets while radical $BrO_2^\bullet$ (or its dimer Br_2O_4) capable of diffusion through the organic phase plays the role of the rapidly diffusing activator. The molecules of $HBrO_2$ and $BrO_2^\bullet$ are coupled through the chemical reactions

$$BrO_3^- + HBrO_2 + H^+ \rightarrow 2BrO_2^\bullet + H_2O\,, \qquad (49)$$

$$\mathrm{cat(red)} + BrO_2^\bullet + H^+ \rightarrow \mathrm{cat(ox)} + HBrO_2\,, \qquad (50)$$

where cat(red) and cat(ox) are the reduced and oxidized forms of the catalyst, respectively.

As a rule, a wave instability appears in the BZ–AOT system at large ϕ_d values close to percolation ϕ_cr and higher than those ϕ_d at which Turing patterns arise. A simple explanation of this fact (even if incomplete, given the complexity of the system) comes from the computation of the Br_2 and $BrO_2^\bullet$ concentrations in the organic phase as a function of ϕ_d. With the concentration of Br_2 or $BrO_2^\bullet$ denoted by x and the subscript 'w' used for the aqueous phase, 'S' for the surfactant phase, and 'oil' for the organic phase, the following material balance equation is obtained:

$$\phi_\mathrm{w} x_\mathrm{w} + \phi_\mathrm{S} x_\mathrm{S} + \phi_\mathrm{oil} x_\mathrm{oil} = \phi_\mathrm{w} x_0\,, \qquad (51)$$

$$\phi_\mathrm{w} + \phi_\mathrm{S} + \phi_\mathrm{oil} = 1\,, \qquad (52)$$

where x_0 is the initial concentration of x in the water phase, $\phi_\mathrm{w} + \phi_\mathrm{S} \equiv \phi_\mathrm{d}$, and $\phi_\mathrm{S} = 21.6\phi_\mathrm{w}/\omega$ [see Eqn (1)]; in our experiments, ω usually equals 15. For $x = [Br_2]$, when the partition coefficients of the phases K_1 and K_2 ($x_\mathrm{w}/x_\mathrm{S} = K_1$, $x_\mathrm{S}/x_\mathrm{oil} = K_2$) are 0.002 and 5, respectively, [93], it is found that x has a maximum at $\phi_\mathrm{d} = 0.3-0.4$. If $x = [BrO_2^\bullet]$ and $K_1 \cong K_2 \cong 0.8-1.0$ (the values estimated from the data for stable radical $ClO_2^\bullet$), x has a maximum at $\phi_\mathrm{d} = 0.5-0.6$. Thus, the wave instability emerges at a maximum concentration of the rapidly diffusing activator ($BrO_2^\bullet$) and the Turing instability at a maximum concentration of the inhibitor (Br_2).

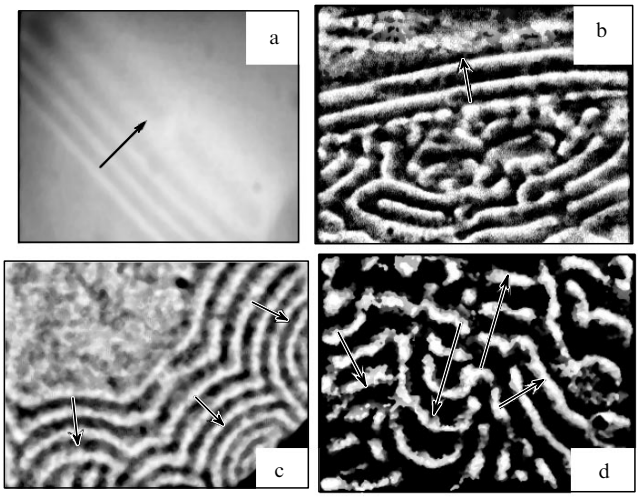

Figure 8. Various forms of wavepackets in the BZ–AOT system: (a) isolated wave packet, (b) wave packet in the form of two long plane waves behind which wave chaos developed, (c) wave packets with negative wave curvature, (d) wave packets traveling in different, including opposite (in the center), directions. Arrows show the directions of wave movements within wave packets. Snapshot (c) displays the edge of the Teflon gasket in the right bottom corner. White and black colours correspond to the maximum and minimum concentrations of the oxidized catalyst (ferriin), respectively. Snapshot size: (a) 2.5×2.2 mm, (b, d) 1.88×1.4 mm, (c) 3.76×2.81 mm. Initial concentrations in the aqueous phase: (a) $[MA]_0 = 0.25$ M, $[H_2SO_4]_0 = 0.2$ M, $[NaBrO_3]_0 = 0.15$ M; (b) $[MA]_0 = 0.3$ M, $[H_2SO_4]_0 = 0.3$ M, $[NaBrO_3]_0 = 0.2$ M; (c) $[MA]_0 = 0.3$ M, $[H_2SO_4]_0 = 0.2$ M, $[NaBrO_3]_0 = 0.23$ M; (d) $[MA]_0 = 0.3$ M, $[H_2SO_4]_0 = 0.3$ M, $[NaBrO_3]_0 = 0.2$ M; [ferroin]$_0 = 0.004$. Parameters of microemulsion ($\omega = [H_2O]/[AOT]$): (a) $\omega = 15$, $\phi_\mathrm{d} = 0.57$; (b, d) $\omega = 16.4$, $\phi_\mathrm{d} = 0.64$; (c) $\omega = 15.2$, $\phi_\mathrm{d} = 0.45$.

6.1 Packet waves

We choose an originally homogeneous system that has a wave instability ($\mathrm{Re}\,\Lambda > 0$ at $\mathbf{k} = \mathbf{k}_\mathrm{w}$ and $\mathrm{Im}\,\Lambda \neq 0$) and a single steady state ($\mathrm{Re}\,\Lambda < 0$ at $\mathbf{k} = 0$). Then, any small local perturbation gives rise to a wave packet. Examples of wave packets observed in the BZ–AOT system [63] are presented in Fig. 8. Unlike trigger waves propagating over the entire system and crossing it from one border to the other, packet

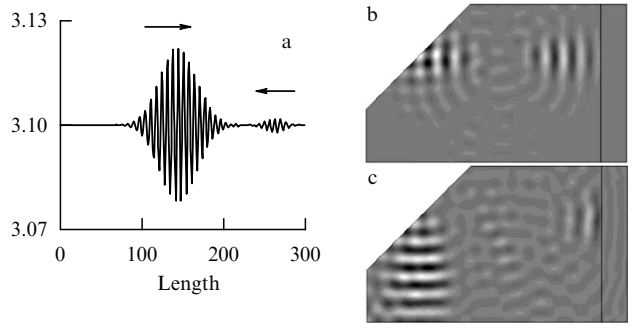

Figure 9. Properties of wave packets: (a) the absence of annihilation upon collision of two wave packets, the packets penetrate each other; (b) specular reflection of wave packets from the surface, with the incidence angle equal to the reflection angle. Computer simulation for the extended Brusselator model:

$$\frac{\mathrm{d}u}{\mathrm{d}t} = \frac{1}{\varepsilon_1}[a - (1+b)u + u^2 v - cu + dw] + D_\mathrm{u}\Delta u\,,$$

$$\frac{\mathrm{d}v}{\mathrm{d}t} = bu - u^2 v + D_\mathrm{v}\Delta v\,, \qquad \frac{\mathrm{d}w}{\mathrm{d}t} = \frac{cu - dw}{\varepsilon_2} + D_\mathrm{w}\Delta w\,.$$

Parameters: $a = 3.1$, $b = 3.2$, $c = 2$, $d = 1.5$, $\varepsilon_1 = 0.02$, $\varepsilon_2 = 0.61$, $D_\mathrm{u} = D_\mathrm{v} = 1$, $D_\mathrm{w} = 20$. Time elapsed since the initial perturbation (dimensionless units); (b) $t = 12$, (c) $t = 26$. Boundary conditions: zero flux. Rectangle size: 100×60.

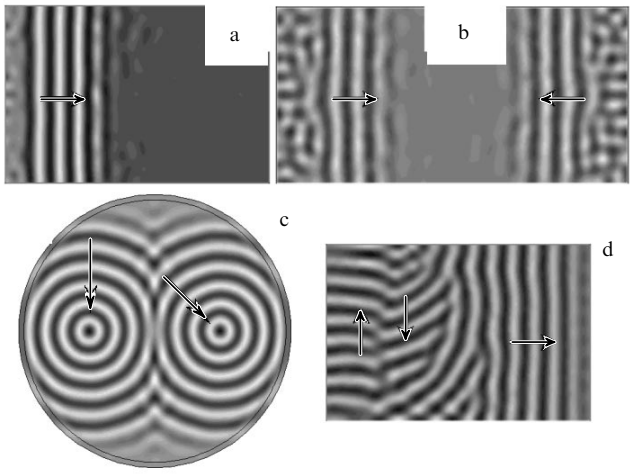

Figure 10. Modelling packet waves with system of equations (39) – (42). System size: (a, d) 150×100, (b) 200×100, (c) $R = 50$. The parameters of the model correspond to the parameters of curve *1* in Fig. 4a for (a), curve *2* in Fig. 4a for (b and d), curve *3* in Fig. 4b for (c). The narrow vertical stripe (of width *l*) was initially perturbed at the left edge in cases (a) and (d) and at either edge in case (b); in case (c), two points initially perturbed on the diameter ($R/2$ from the center) later became the centers of inwardly propagating phase waves. Conversion to the dimensional unit length in centimeters is effected by multiplying the dimensionless units by $(10^{-5}/k_5)^{1/2}$, where $k_5 \cong 1$.

waves, which are actually phase waves, can propagate only inside a given packet. Figure 8a shows a wave packet and two unperturbed regions, in the bottom left and top right corners. The waves travel only inside the packet and gradually disappear at its edges, failing to reach the unperturbed zone in the top right corner. This is the first experimental demonstration of packet waves in a chemical system. Another example is presented in Fig. 8b. In a packet of two long (horizontal) waves, they travel rapidly, but the packet itself is practically motionless. Chaotic waves can be seen behind the packet.

Similarly to packet waves in optics and acoustics, two wave packets can penetrate each other. A collision of two wave packets in a chemical reaction – diffusion system was simulated on a computer in the early studies of wave instability [66]. However, the results of this work did not clarify whether the waves passed through each other or were reflected. Knowing that standing waves arose in the zone where the two packets collided, it was natural to suggest that the waves penetrated each other. But the definitive answer was obtained quite recently [116] using a model with two different wave packets (Fig. 9a). It was shown that the large and the small packets changed places after collision, that is, penetrated each other. The movement of the wave packets in opposite directions within practically the same spatial area observed in experiment is depicted in Fig. 8d.

In the case of negative dispersion ($\mathrm{d}\,\mathrm{Im}\,\Lambda/\mathrm{d}k < 0$, see Fig. 4b), packet waves have negative curvature and propagate towards the perturbation center (Fig. 8c). This may look like a violation of the causality principle: the effect (waves) moves backward to the cause (the initial local perturbation of the system; in the experiment depicted in Fig. 8c, perturbation is represented by the reactor wall). This apparent discrepancy can be understood bearing in mind that in the case of wave packets, the information generated by the perturbation is carried by the entire packet rather than the individual phase waves, and the result is the packet itself, not the waves. The packet as a whole always propagates away from the perturbation center. The group velocity of the packet defined as $|\mathrm{d}\,\mathrm{Im}\,\Lambda/\mathrm{d}k|$ at $\mathbf{k} = \mathbf{k}_\mathrm{w}$, where $\mathrm{Re}\,\Lambda$ has a maximum, is always positive. The absolute velocity of phase waves is $\mathrm{Im}\,\Lambda/k$ at $\mathbf{k} = \mathbf{k}_\mathrm{w}$, and their direction is given by the sign of $\mathrm{d}\,\mathrm{Im}\,\Lambda/\mathrm{d}k$ at $\mathbf{k} = \mathbf{k}_\mathrm{w}$.

It was possible to simulate all the experimentally available types of wave packets presented in Fig. 8 using the system of equations (39) – (42). The results are shown in Fig. 10. Each frame in this figure is to be compared with the corresponding snapshot in Fig. 8.

6.2 Antispirals

In the BZ – AOT system with negative dispersion ($\mathrm{d}\,\mathrm{Im}\,\Lambda/\mathrm{d}k < 0$ at $\mathbf{k} = \mathbf{k}_\mathrm{w}$), there arise antispirals and antipacemakers [117] — new types of spiral (or concentric) waves directed towards the center (Fig. 11) [62, 63]. The spiral frequency for all experimentally found antispirals is lower than the bulk oscillation frequency ω_0 ($\omega_0 = \mathrm{Im}\,\Lambda$ at $\mathbf{k} = 0$). Antispirals also occur when a point system (the same system in a well-mixed reactor) is in a steady state, i.e., undergoes no oscillations.

It has been shown in a recent theoretical work [118] that the complex Ginzburg – Landau equation may also yield antispirals and antipacemakers. For this, as in our experiment [62], the frequency of system oscillations ω_0 at $\mathbf{k} = 0$ (bulk oscillations) must be higher than the frequency ω_w at $\mathbf{k} = \mathbf{k}_\mathrm{w}$. It follows that antispirals can also be found in ordinary homogeneous systems with two variables of the activator – inhibitor type, when the diffusion coefficients of the activator and the inhibitor are identical. In other words, wave instability is not indispensable for discovering antispirals. However, they have not thus far been reported to occur in homogeneous systems. Moreover, we have demonstrated that ordinary, outwardly propagating phase waves emerge if $\omega_0 > \omega_\mathrm{w}$ but $\mathrm{d}\,\mathrm{Im}\,\Lambda/\mathrm{d}k > 0$ (Fig. 2b, d in [63]).

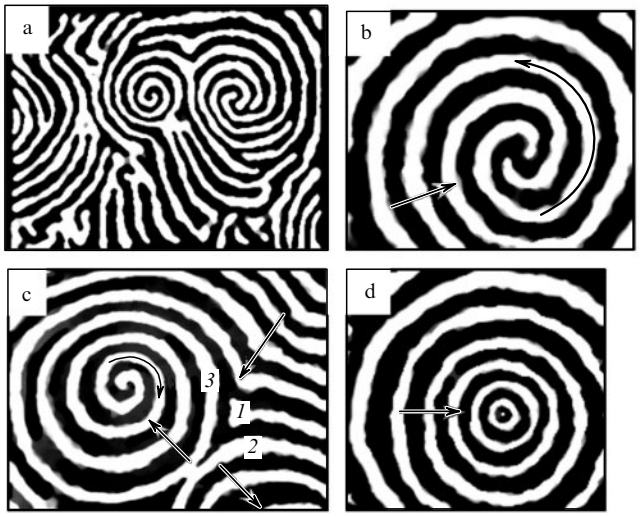

Figure 11. Antispirals (a–c) and antipacemakers (d) in the BZ–AOT system. Parameters of microemulsion: (a–c) $\phi_d = 0.55$, (d) $\phi_d = 0.59$. Initial concentrations of the reactants in the aqueous phase: $[MA]_0 = 0.3$ M, $[H_2SO_4]_0 = 0.2$ M, [ferroin]$_0 = 4$ mM, $[NaBrO_3]_0 = 0.23$ M (a), 0.2 M (b, c), 0.21 M (d). Snapshot size: (a) 5.1×3.75 mm, (b) 1.8×1.5 mm, (c) 3×2.25 mm, (d) 2.7×2.5 mm. Arrows show the direction of wave propagation and antispiral rotation.

Antispirals, or more generally, spiral waves with the negative curvature moving toward the core of the spiral, are more widespread than wave instability with negative dispersion. The first example of short-lived (unstable) antispirals obtained in a numerical experiment [119] is provided by trigger waves in a model of the FitzHugh–Nagumo type (with two variables). The source of these waves was located in the corners of a small square (zero fluxes at the boundaries) and served as an external source of oscillations with respect to the antispiral. It should be noted that, in this case, the frequency of the 'external' source was also higher than that of the antispiral. In this model, waves propagate away from the perturbation source. A similar explanation of antispirals based on the concept of trigger waves was offered in our first publication in *Science* [62], where I managed to simulate a stable rotating antispiral. In the case of wave instability with negative dispersion and in our experiment with the BZ–AOT system, phase packet waves propagate towards the perturbation source coincident with the core of the spiral [63].

In 2003, a few works were published almost simultaneously dealing with antispirals found in totally different systems [118, 120–122]. They mark the beginning of investigations into these phenomena.

6.3 Reflection of wave packets

Unlike trigger waves, which as a rule die upon collision with a nontransparent surface (zero flux at the boundary), the mechanisms of reflection of wave packets, in a way, obey geometric optics laws, namely, the reflection angle is exactly equal to the incidence angle (Fig. 2b, c) [71]. Packet waves propagating along a narrow capillary tube whose diameter is smaller than the wavelength may be partly reflected at the site where the tube opens into a much wider space filled with the same reaction system and partly pass through this region [71]. The reflection/transmission coefficient depends on the capillary diameter. Such behavior of wave packets resembles properties of a semitransparent mirror in optics. At such a geometry, a trigger wave dies as it leaves the capillary tube [123, 124] if its radius is smaller than the critical radius $r_{cr} = D/v_0$, where v_0 is the plane wave velocity and D is the activator diffusion coefficient.

6.4 Standing waves

In the course of time, packet waves transform into standing waves as a result of interaction with other wave packets. Typical standing waves found in the BZ–AOT system [61] are shown in Fig. 12. The patterns presented in Figs 12b and 12d correspond to two antiphases (the time interval between the two snapshots is $T/2$) whereas snapshot 12c is obtained after time T (approximately 2 min following the snapshot 12b). Summation (or superposition) of snapshots 12b and 12c (Fig. 12e) gives evidence that the structures do not substantially change for time $t = T$. Summation of photos 12b and 12d (Fig. 12f) results (after time $T/2$) in the replacement of black spots by white ones and vice versa. This is typical behavior of standing waves for which there must exist nodes not changing in time; in our case, these are lines at the borderline between the white and black spots. The characteristic wavelength of standing waves is around 0.2 mm.

Numerical computation of model (39)–(42) with wave instability yields regular structures periodically changing in time (Fig. 13a–j) within a small spatial area (some four wavelengths). If the size of this region is considerably larger (as in Fig. 13k), the standing waves look like those in experiments.

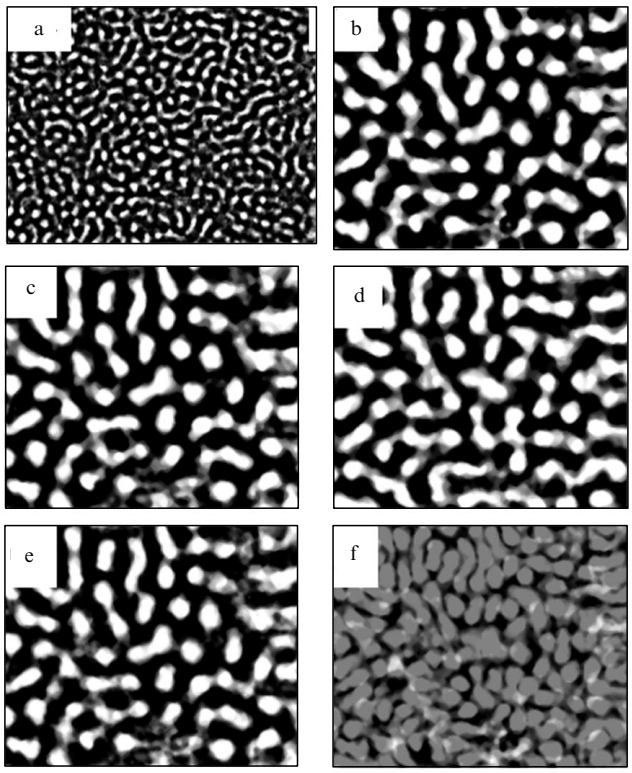

Figure 12. Standing waves in the BZ–AOT system: (a) snapshot size 5×3.7 mm; (b–d) small fragment of the standing wave shown in figure (a) (size: 1.9×1.4 mm) at time moments $t = 0$ (b), $T/2$ (d), T (c); (e) the result of summation of the waves shown in figures (b) and (c); (f) the same for figures (b) and (d). Parameters of the BZ–AOT system: $\omega = 15$, $\phi_d = 0.473$, $[MA]_0 = 0.4$ M, $[H_2SO_4]_0 = 0.2$ M, $[NaBrO_3]_0 = 0.18$ M, [bathoferroin]$_0 = 5$ mM.

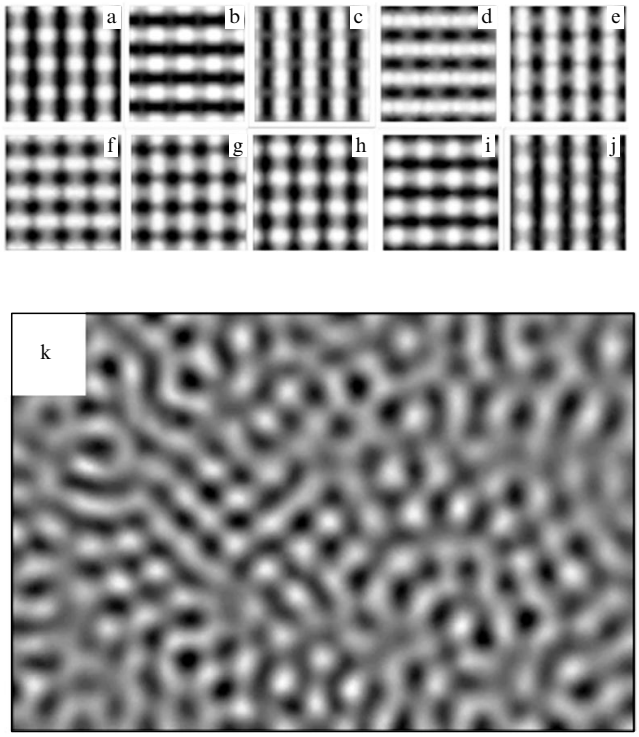

Figure 13. Standing waves in model (39)–(42): (a–j) the full cycle of standing waves at equal time intervals $T/8$. Parameters of the model for the (a–j) series $q = 4 \times 10^{-4}$, $f = 1.5$, $\varepsilon = 0.3$, $\varepsilon_2 = 1.5$, $\varepsilon_3 = 0.003$, $\alpha = 0.3$, $\beta = 0.26$, $\gamma = 0.4$, $\chi = 0$, $D_x = D_z = 0.01$, $D_s = D_u = 1$; size 20×20. Parameters of the model for (k): $q = 3 \times 10^{-3}$, $f = 1.5$, $\varepsilon = 0.385$, $\varepsilon_2 = 3.2$, $\varepsilon_3 = 0.0024$, $\alpha = 6.3$, $\beta = 0.275$, $\gamma = 0.1$, $\chi = 0.004$, $D_x = D_z = 0.01$, $D_s = D_u = 1$; size 150×100.

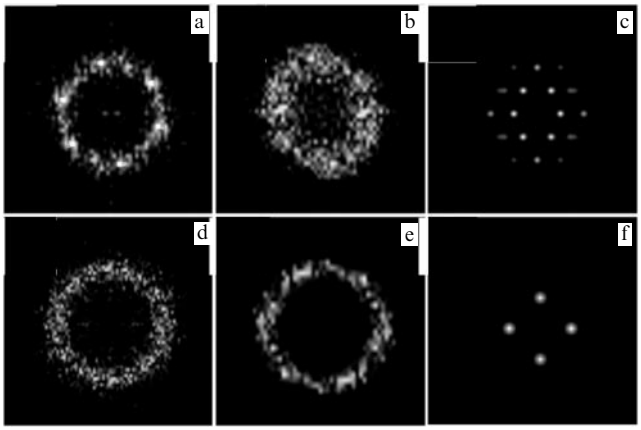

Figure 14. 2-D-Fourier transform of: (a) Turing patterns in Fig. 5a, (b) Turing labyrinthine patterns in Fig. 5c, (c) hexagonal Turing structure in Fig. 5d, (d) standing waves in Fig. 12a, (e) in Fig. 13k and (f) in Fig. 13g.

Figure 14 compares two-dimensional Fourier transformation of standing waves and Turing patterns in experiment and in model (39)–(42). It can be seen that the Fourier transform of hexagonal Turing structures (shown in Fig. 5d) has six well-apparent peaks (Fig. 14c) in contrast to that of standing waves depicted in Fig. 13a–j, which have four peaks (Fig. 14f). At different time moments corresponding to snapshots 13a–j, the amplitudes of the four peaks in Fig. 14f change, while their position remains unaltered. In the Fourier transform (Fig. 14a) of experimental Turing patterns (shown in Fig. 5a), the six characteristic peaks are difficult but possible to distinguish.

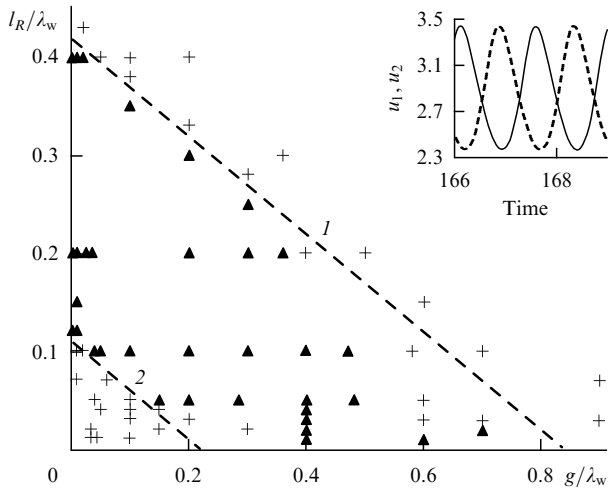

Figure 15. Parametric diagram for heterogeneous system (53)–(58). Triangles and plus signs denote antiphase oscillations and steady state, respectively. $L/\lambda_w = 0.84$ for line *1* and $L/\lambda_w = 0.22$ for line *2*, $\lambda_w = 2\pi/k_w = 17.923$, $2l_R + g \equiv L$. The inset shows typical out-of-phase oscillations of the variable u at $l_R/\lambda_w = 0.3$ and $g/\lambda_w = 0.01$, where u_1 and u_2 are concentrations in the midst of the practically homogeneous left and right droplets respectively (see Fig. 6a for droplets). Parameters: $a = 2.85$, $b = 11$, $c = 2$, $d = 5$; between droplets $D_u = D_v = 0$, $D_w = 100$, inside droplets $D_u = D_v = D_w = 100$.

6.5 Standing waves in a heterogeneous system

We consider two water droplets (shown in Fig. 6a) embedded in a nonaqueous (organic) phase as an elementary structure of the heterogeneous system. Let the droplets contain (as before) a dynamical system described, for instance, by the Brusselator model. Furthermore, let the signal molecule (w), able to diffuse in the interdroplet space, be linearly related to the activator such that the total system is described by the equations

$$\frac{\partial u}{\partial t} = a - (1 + b)u + u^2 v - cu + dw + D_u \frac{\partial^2 u}{\partial x^2}\,, \tag{53}$$

$$\frac{\partial v}{\partial t} = bu - u^2 v + D_v \frac{\partial^2 v}{\partial x^2}\,, \tag{54}$$

$$\frac{\partial w}{\partial t} = cu - dw + D_w \frac{\partial^2 w}{\partial x^2}\,, \tag{55}$$

where $D_u = D_v = D_w$ in the droplets and $D_u = D_v = u = v = 0$ in the gap between them. Let the parameters a, b, c, and d be chosen such that the only steady state of system (53)–(55) is stable for an isolated droplet ($\mathrm{Re}\,\Lambda < 0$ at $\mathbf{k} = 0$). A system of two drops may lose stability and give rise to antiphase oscillations at given spatial sizes of the droplet (l_R) and the gap (g) [110]. Such an outcome, illustrated by Fig. 15, results from the wave instability that arises in the two-droplet system coupled via messenger w, which is in turn chemically coupled to the activator. The wavelength of the wave instability is then equal to two lengths of the entire system, i.e., $4l_R + 2g$. Therefore, the sum $4l_R + 2g$ must correspond to wave numbers at which $\mathrm{Re}\,\Lambda > 0$. This condition determines the region l_R and g in Fig. 15 where out-of-phase oscillations occur.

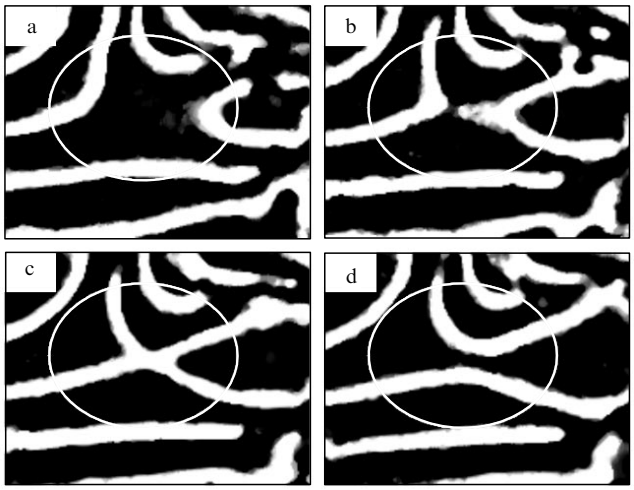

Figure 16. Accelerating waves in the BZ–AOT system. Initial concentrations in the aqueous phase: $[H_2SO_4]_0 = 0.2$ M, $[NaBrO_3]_0 = 0.15$ M, $[MA]_0 = 0.3$ M, [ferroin]$_0 = 4$ mM; $\omega = 18.8$, $\phi_d = 0.74$, $t = 90$ s (a), 110 s (b), 122 s (c), 134 s (d). Ellipses outline zones in which two waves are accelerated prior to collision. Size: 5.2×4.0 mm.

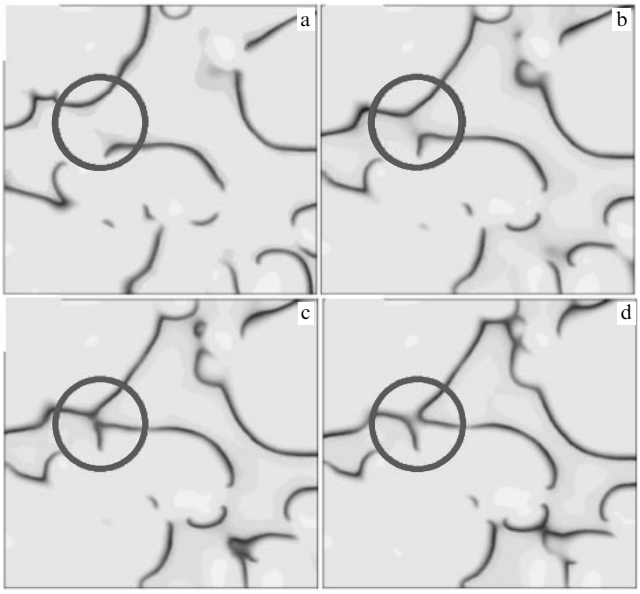

Figure 17. Accelerating waves in the extended Brusselator model described in captions to Fig. 9. Parameters: $a = 2.9$, $b = 3.2$, $c = 2$, $d = 1.5$, $\varepsilon_1 = 0.02$, $\varepsilon_2 = 0.2$, $D_u = D_v = 1$, $D_w = 20$. Size: 30×30, $t = 1.126$ (a), 1.146 (b), 1.156 (c), 1.166 (d). The circle in each figure is intended to draw attention to two accelerating waves.

6.6 Accelerating waves

When the volume fraction of water nanodroplets in a microemulsion exceeds the percolation threshold, accelerating waves may be generated [61]. Two waves approaching each other (Fig. 16) gradually accelerate and their curvature increases (the waves become sharp-pointed), in contradiction with the known equation that relates the velocity and the curvature of the trigger wave as [125, 126]

$$v = v_0 - \frac{1}{r} D\,, \tag{56}$$

where v_0 is the plane wave velocity, D is the diffusion coefficient, and r is the wave arc radius ($1/r$ is the curvature). In accordance with Eqn (56), increasing $1/r$ must decelerate the wave. But experiment gives the opposite picture, that is, the wave velocity increases considerably (several-fold). When the waves come sufficiently close to each other, a small bridge is formed to connect them (Fig. 16b). The waves do not annihilate after collision as ordinary trigger waves do; instead, they seem to 'flip-flop' and diverge in the perpendicular direction (Fig. 16d).

This phenomenon was explained by the influence of a fast diffusing activator ($HBrO_2^{\bullet}$), whose concentration in front of the wave may be very high. As the two waves approach each other, the concentration of $HBrO_2^{\bullet}$ between them may at least double, leading to autocatalysis, and hence to wave acceleration. We reproduced this phenomenon [71] using an extended Brusselator model of type (53)–(55). The results of modeling (Fig. 17) are in good agreement with experimental observations.

7. Segmented waves and spirals

It follows from Fig. 3 that freshly prepared microemulsions containing reagents of the BZ reaction exhibit a bimodal droplet distribution by size. Earlier studies of BZ–AOT systems [58–60, 127] have demonstrated that chemical reaction rate constants depend on the size of water droplets. Therefore, the BZ reaction should proceed differently in different pools, i.e., in the presence of droplets of different size. Such a system can be represented as two diffusely coupled subsystems having certain (not measured in experiment) constants of mass exchange between them that may differ for different reactants (k_x and k_z):

$$\frac{\partial x_1}{\partial \tau} = \frac{1}{\varepsilon_1}\left(x_1 - x_1^2 + f_1 z_1 \frac{q_1 - x_1}{x_1 + q_1}\right) - \phi k_x (x_1 - x_2) + D_{x_1} \Delta x_1\,, \tag{57}$$

$$\frac{\partial x_2}{\partial \tau} = \frac{1}{\varepsilon_2}\left(x_2 - x_2^2 + f_2 z_2 \frac{q_2 - x_2}{x_2 + q_2}\right) - k_x (x_2 - x_1) + D_{x_2} \Delta x_2\,, \tag{58}$$

$$\frac{\partial z_1}{\partial \tau} = x_1 - z_1 - \phi k_z (z_1 - z_2) + D_{z_1} \Delta z_1\,, \tag{59}$$

$$\frac{\partial z_2}{\partial \tau} = x_2 - z_2 - k_z (z_2 - z_1) + D_{z_2} \Delta z_2\,. \tag{60}$$

At certain parameters, model (57)–(60) may have three steady states. As a rule, the mid-state is an unstable saddle. Two other states may be of different stability types. If one (main) state is stable but excitable (i.e., readily responds to a supercritical perturbation) while the other displays the instability that we call the pseudo-Turing instability [64] (see below), system (57)–(60) describes a surprising type of wave referred to as dash or segmented waves [64, 81].

These waves have been discovered in experiment as plane, concentric, and spiral, shown in Fig. 18. All spiral waves found to date in chemical and physical systems are smooth waves.[2] Only a few biological entities, such as seashells, lichens, and pine cones have been found to exhibit segmenta-

[2] Breaking chaotic waves in the BZ reaction were first observed 20 years ago in an open reactor as a result of interaction between smooth chemical waves and hydrodynamic Benard convections that arise from cooling of the upper layer due to evaporation [165]. Both the wave-breaks and the Benard convection cells disappear as soon as the reactor (Petri dish) is covered with a piece of glass. In our case, the reactor is closed and there are no hydrodynamic flows in it.

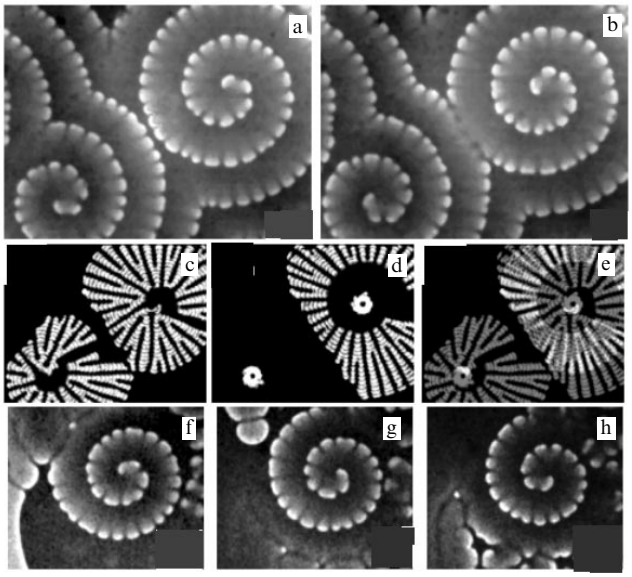

Figure 18. Segmented spirals in the BZ – AOT system. (c – e) segment trajectories of the spiral shown in snapshots (a, b); Δt between snapshots (a) and (b) is 66 s, between (f) and (g) 219 s, and between (g) and (h) 244 s; (a, b) well developed and (f – h) arising segmented spirals at different ϕ_d: $\phi_d = 0.36$ (a, b), 0.47 (f – h). Concentrations of reagents: $[MA]_0 = 0.3$ M, $[H_2SO_4]_0 = 0.2$ M, $[NaBrO_3]_0 = 0.18$ M, [bathoferroin] = 0.0049 M; $\omega = 15$. Stroboscopic pictures (c) and (d) were obtained by the superposition of snapshots taken every 50 s. Figures (c) and (d) were made using only segments of a single spiral coil, initially the first (closest to the spiral core) and the second ones, for (c) and (d), respectively. The two 'white eyes with black pupils' in figure (d) were obtained by the superposition of snapshots in which only one spiral segment was retained (closest to the core in all time moments). Figure (e) was obtained by the superposition of snapshots (c) and (d). White color corresponds to the overlapping white colors in (c) and (d). Snapshot size: (a – e) 3.72 × 4.82 mm, (f – h) 2.11 × 2.63 mm.

tion of these patterns. One more example of segmented spirals in living nature is provided by phyllotaxis or the arrangement of leaves on a stem of certain plants [128]. Therefore, segmented spirals discovered in chemical systems may be of importance for biology, e.g., for understanding morphogenesis.

The physics of these spirals consists of the combination of incompatibles: propagating trigger waves and stationary 1-D Turing patterns. The key role is played by the pseudo-Turing instability or, in other words, by a Turing-like instability [64, 81] that (similarly to the usual Turing instability) has a positive maximum of the real part $\mathrm{Re}\,\Lambda$ of the eigenvalue of the characteristic equation at a nonzero wave number $\mathbf{k}_T$. This $\mathbf{k}_T$ value determines the characteristic size of the segment + gap unit as $2\pi/k_T = \lambda_T = 0.28 - 0.3$ mm. The Turing-like instability is distinct by positive $\mathrm{Re}\,\Lambda$ at $\mathbf{k} = 0$, which suggests global instability of this steady state (the third one in our case). For the ordinary Turing instability, $\mathrm{Re}\,\Lambda < 0$ at $\mathbf{k} = 0$ and the steady state retains stability in response to a homogeneous perturbation.

At a certain spatial point in the reactor with segmented waves, the system switches from the ground state to the excited one due to the subcritical perturbation induced by a segment of the same spiral approaching this point. The space between the segments does not undergo excitation (at least not strongly) because it is dominated by the inhibitor that has a higher diffusion coefficient (as in the cases of the ordinary Turing instability). After a lapse of time, all the excited points return to the initial stable state as a result of global instability of the excited (third steady) state. If in this case $\mathrm{Re}\,\Lambda$ at $\mathbf{k} = 0$ were negative (as in the ordinary Turing instability), then the resulting Turing patterns might be stable and we could see the spreading front that leaves stationary Turing structures behind. But in our case, they disappear and the system switches over to the unexcited but excitable homogeneous steady state.

Segmented spirals arise only from smooth ordinary spirals that must be generated in the system in advance as basic pattern-forming structures. If concentric waves instead of spirals are present in the system, segmented concentric (rather than spiral) waves emerge as soon as the conditions for wave segmentation mature (in a closed system, concentrations of reagents and intermediates slowly change with time). When segmentation occurs, the velocity of all waves (spiral, plane, and concentric) sharply decreases (approximately 2 – 3-fold). In a theoretical study of Turing patterns propagating under the effect of an external locally propagating excitation, we have demonstrated that the translational movement of Turing patterns is possible only at a small propagating velocity of this external excitation [129].

As segments of a spiral move away from the center, they grow in size until a certain critical value: then each segment splits into two new ones, as can be seen from their trajectories in Figs 18c – e. The gaps between the segments remain unaltered.

In one-day-old microemulsions, where the droplet distribution by size is close to monomodal, dash waves and segmented spirals have never been observed.

Replicating spots distantly reminiscent of segmented spirals have been found in a ferrocyanide – iodate – sulfite system [130] and simulated in the Gray – Scott system [131] that can also have three steady states, with the mid-state being an unstable one. There are no reports on the detailed comparison of these systems and a model system in which localized impulses/waves travel as a regular group [132].

8. Localized patterns. Oscillons

In the preceding section, we considered a situation in which a system had a few (three) steady states. The present section is focused on a spatially extended system that can exist in either a steady or an oscillatory state with the same parameters. It is well known from the theory of oscillations in point (0-D) dynamical systems that the steady state may lose stability in two modes, supercritical and subcritical, through the mechanism of the Andronov – Hopf instability [133, 134]. In the latter case (rigid excitation of oscillations), there is a range of parameters at which the system can exist in two states, stationary and oscillatory, depending on the initial conditions.

A spatially extended system with one steady state and the Turing instability can also lose its homogeneous steady state in two different ways, supercritical and subcritical [135, 136]. In a certain narrow range of parameters of spatially extended systems, localized stationary Turing patterns are then likely to arise, as in the models reported in Ref. [136]. What does occur in a system when the Turing and Andronov – Hopf subcritical bifurcations are realized simultaneously?

We begin with experiments in the BZ – AOT system catalyzed by metallocomplexes $Ru(bpy)_3^{2+}$. Not far from the steady state – oscillation boundary and at ϕ_d below the percolation threshold, the entire system exhibits stationary

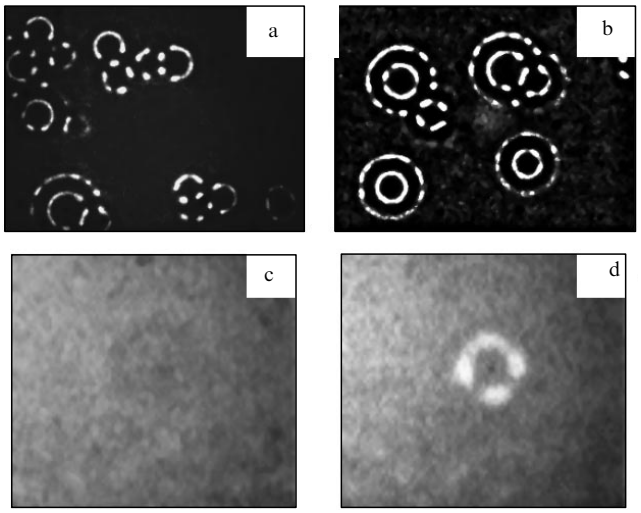

Figure 19. Localized Turing patterns (a,b) and oscillon in two antiphases (c, d) in the BZ–AOT system catalyzed by $Ru(bpy)_3^{2+}$. Snapshots (a, b) were taken in different reaction zones. The oscillon period of the oscillon is 47 s, the outer diameter about 0.6 mm. Parameters of the system:

$\phi_d = 0.41$, $\omega \equiv [H_2O]/[AOT] = 15$, $[H_2SO_4]_0 = 0.25$ M,
$[NaBrO_3]_0 = 0.2$ M, $[MA]_0 = 0.25$ M, $[Ru(bpy)_3^{2+}]_0 = 4.2$ mM.

Snapshot size: (a, b) 5.06×3.73 mm, (c, d) 2.13×1.87 mm.

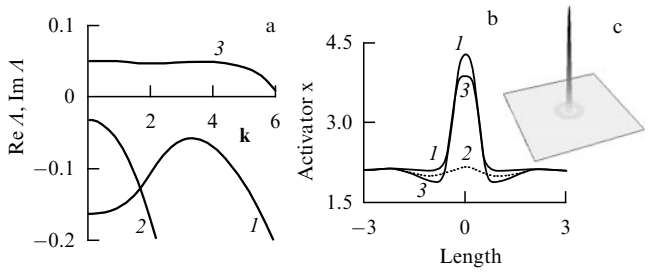

Figure 20. Oscillon in the 2-D model (61)–(63). (a) Dispersion curves: *1* — real eigenvalue of the characteristic equation, *2* ($\mathrm{Re}\,\Lambda$) and *3* ($\mathrm{Im}\,\Lambda$) — complex eigenvalue of the characteristic equation; curve *3* is $\mathrm{Im}\,\Lambda/6$; (b) *1*, *2* — oscillon cross section, *3* — cross section of the stationary localized Turing peak; (c) — stereo view of the oscillon at its maximum, size: 20×20. Parameters of the model: $k_1 = 2.1$, $k_2 = 1$, $K = 3.4$, $k_4 = 1.8$, $k_5 = 0.47$, $k_6 = 0.05$, $k_7 = 0.6$, $k_8 = 0.14$, $D_x = D_z = 0.01$, $D_y = 0.035$. The maximum of curve *1* becomes positive with increasing D_y (the subcritical Turing bifurcation); the maximum of curve *2* at $\mathbf{k} = 0$ becomes positive with increasing k_5 (the subcritical Andronov–Hopf bifurcation).

structures similar to Turing patterns (Fig. 19a, b). But unlike the structures shown in Fig. 5, they do not occupy the total reaction area but remain localized. Obviously, in this case, we are dealing with the subcritical Turing instability. The centers of these localized concentric Turing patterns are likely to harbor microscopic dust particles that play the role of local suprathreshold perturbations of the homogeneous state. After a lapse of 0.5–1 hours, these localized structures begin to oscillate. The behavior of an individual structure remote from other patterns is illustrated by Figs 19c, d. Following Umbanhowar and co-workers [48], who discovered small localized oscillations in a layer of periodically vibrated sand, we name these patterns oscillons. It should be noted that in our case the system experiences no external influence.

We tried to explain the origin of oscillons by a combination of the subcritical Turing and Andronov–Hopf bifurcations. Model (39)–(42) allows us to find parameters at which the system simultaneously exhibits the subcritical Turing instability (giving rise to localized Turing structures as in Fig. 19a, b) and the subcritical Andronov–Hopf instability (at $f < 1 - q$). However, the combination of these instabilities yields no oscillons; instead, all localized perturbations lead to localized stationary Turing patterns in both the 1-D and 2-D cases.

Oscillons were obtained in other reaction–diffusion models, including a more realistic (and more complicated) model that describes the BZ–AOT system [137] and a model describing oscillations of Ca^{2+} ions inside the cell [137–139]:

$$\frac{dx}{dt} = k_1 - k_2 x - k_4 x + \frac{k_5 y x^4}{K^4 + x^4} + k_6 y - k_7 x + k_8 z + D_x \Delta x, \tag{61}$$

$$\frac{dy}{dt} = k_4 x - \frac{k_5 y x^4}{K^4 + x^4} - k_6 y + D_y \Delta y, \tag{62}$$

$$\frac{dz}{dt} = k_7 x - k_8 z + D_z \Delta z. \tag{63}$$

Typical dispersion curves for model (61)–(63) with an oscillon are presented in Fig. 20a and the oscillon itself with its cross section in Figs 20b, c. Figure 20a shows that the real parts of the eigenvalues of the characteristic equation are negative at all wave numbers. The appearance of the oscillon in the model is due to the nonlinear interactions between the oscillatory mode (curve *3* in Fig. 20a) and the spatial Turing instability of the subcritical type (curve *1*). In two different models, oscillons are observable only when the real eigenvalue (curve *1* in Fig. 20a) has a maximum at those **k** values at which the other pair of eigenvalues remains complex coupled, i.e., when $\mathrm{Im}\,\Lambda$ (curve *3*) is not zero.

When model (61)–(63) has the parameters shown in Fig. 20, the oscillon, localized stationary structures, Turing patterns occupying the entire space, homogeneous (bulk) oscillations, and steady state can be realized in the system. The situation depends on the initial perturbations of the original homogeneous state. It can be seen in Fig. 20b that the steady peak (curve *3*) does not significantly differ from the oscillon at its maximum (curve *1*). This accounts for the high sensitivity of the system to an initial perturbation.

The sensitivity of the system to perturbations and the possibility of fixing (remembering) initial perturbations in the form of a stationary or oscillatory peak (a chain of N peaks may be in 2^Nstates) make this system attractive for the creation of a chemical computer in which parallel processing and storage of information are feasible. If the system is perturbed by a rectangular impulse shown in the inset within Fig. 21a, the response depends on the spatial size of the impulse l_p; it may be either a steady peak, an oscillon, or the initial steady state (Fig. 21a).

If the system is perturbed by two identical impulses at a time, the numerous consequences of this perturbation shown in Figs 21c, d depend on both l_p and the gap between the impulses g (see the inset in Fig. 21c). If $g > 2.5\lambda_T$ (where $\lambda_T = 2\pi/k_T$ is the characteristic Turing size, with $\mathbf{k}_T$ corresponding to the maximum of curve *1* in Fig. 20a), the impulses do not practically interact and the behavior of the two peaks (stationary or oscillatory) being formed depends on the impulse width l_p alone. If $g < 2.5\lambda_T$, we can speak about information processing by a nonlinear system. Depending on g, either a homogeneous steady state or patterns with one, two

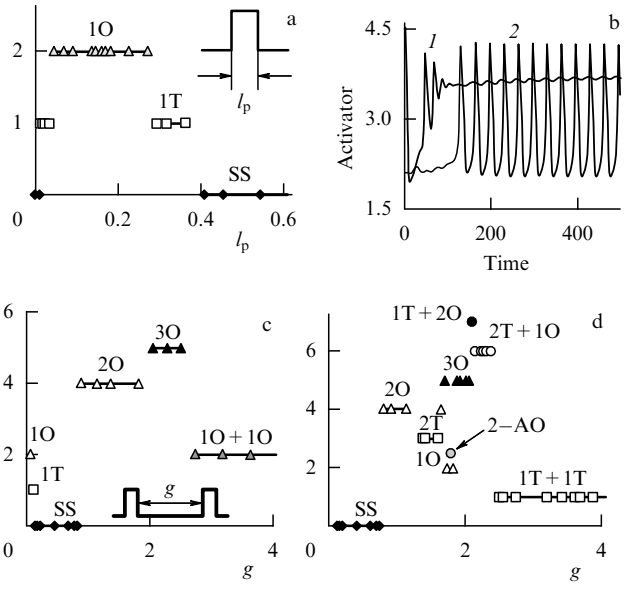

Figure 21. Dependence of the behavior of the 1-D system (61) – (63) on the initial perturbation: (a) perturbation in the form of a solitary rectangular impulse of width l_p, where l_p is measured in units of λ_T (λ_T is the characteristic size of Turing patterns), (c, d) perturbation in the form of two identical impulses of width l_p separated by a gap g also measured in units of λ_T; $l_p = 0.09\lambda_T$ for (c) and $l_p = 0.34\lambda_T$ for (d). Parameters of the model: $k_1 = 2.1, k_2 = 1, K = 3.4, k_4 = 1.8, k_5 = 0.44, k_6 = 0.05, k_7 = 0.6, k_8 = 0.14$, $D_x = D_z = 0.01$, $D_y = 0.06$. Abbreviations: SS — single state (zero value is arbitrarily ascribed to the ordinate), 1T — single stationary Turing peak (ordinate is given a value of 1), 1O — single oscillon (value 2), 2T — Turing pattern with two peaks (value 3), 2O — oscillon with two in-phase peaks (value 4), 3O — oscillon with three in-phase peaks (value 5), 2-AO — oscillon with two out-of-phase peaks (value 2.5), 2T + 1O — three-peak structure: middle peak — oscillations, two others are stationary (value 6), 1T + 2O — three-peak structure: left peak is stationary, two others are in-phase oscillations (value 7), 1T + 1T — two identical weakly interacting Turing peaks, 1O + 1O — two identical weakly interacting oscillons. (b) Temporal behavior of structure 2T + 1O ($g = 2.35\lambda_T = 5.2$), curve *1* — side peak, curve *2* — middle peak; small oscillations of the steady peak are induced by oscillations of the middle peak.

or three peaks can form, both steady and oscillatory. If the resulting structure has a single peak (steady or oscillatory), we can speak about an inhibitory interaction of two impulses and, in the case of a three-peak structure, about activating interaction between two impulses. This situation parallels activating and inhibitory interactions between neurons in the nervous system.

In discussing subcritical bifurcations in reaction – diffusion systems, a natural question arises regarding the feasibility of the subcritical wave instability. We have managed to construct the first model system in which this instability was found. It was the same model (39) – (42) for the BZ – AOT system (the parameters of the model are given in captions to Fig. 22). In this model, the wave instability emerges rigorously, i.e., with an initially large wave amplitude. The system retains the previously formed standing waves in a narrow range of parameters where the maximum of the real part of the eigenvalue becomes negative (see Fig. 22). Such behavior suggests the possibility of oscillon-like localized oscillatory patterns, which have so far not been found in the model. At a small positive maximum value of $\mathrm{Re}\,\Lambda$ and the linear size of the system $L < v_{gr}/\mathrm{Re}\,\Lambda$, the system exhibits high-amplitude soliton-

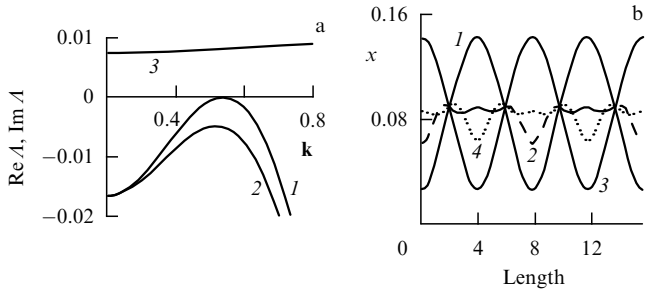

Figure 22. Subcritical wave stability. (a) Dispersion curves: *1* and *2* — $\mathrm{Re}\,\Lambda$, *3* — $\mathrm{Im}\,\Lambda/100$. (b) Standing waves at $\mathrm{Re}\,\Lambda < 0$ [curve *2* in (a)]: *1* — $t = 0$ or T, *2* — $t = T/4$, *3* — $t = 2T/4$, *4* — $t = 3T/4$, $T = 13.81$. Parameters of model (39) – (42): $q = 0.002$, $f = 0.92$, $\varepsilon = 0.309$, $\beta = 0.4$, $\varepsilon_2 = 1.2$, $\alpha = \gamma = \chi = 0$, $D_x = D_z = 0.1$, $D_s = 0.3912$ (curve *1*), 0.36 (curve *2*).

like packet waves that do not change their shape while traveling (with the group velocity $v_{gr} = \mathrm{d}\,\mathrm{Im}\,\Lambda/\mathrm{d}k$ at $\mathbf{k} = \mathbf{k}_w$) [137].

There is a criterion (certain rather complicated analytical functions) that permits one to determine what type of Andronov – Hopf bifurcation (super- or subcritical) exists in a given model, without computer integration of ODE [133]. To date, no similar criterion is known for the wave instability.

9. Clusters. Global negative feedback

Reaction – diffusion systems are known to harbor one more type of nonequilibrium structure, called oscillatory clusters and realized in oscillatory systems that are periodically influenced from the outside [78 – 80, 140 – 144]. Clusters resembling standing waves have no characteristic spatial wavelength. Their shape is normally determined by the initial conditions, but in certain cases (chaotic clusters [78, 79]) may be independent of them.

In terms of organization of external periodic perturbations, all the systems under consideration are categorized into autonomous ones, in which an integrated signal from the entire reaction – diffusion system governs uniform inhibitory effects (as a rule exerted by light on a photosensitive system), and nonautonomous ones, in which a periodic perturbation has its own frequency [146, 147]. For autonomous systems, it is possible to introduce a delay line between the integrated signal from the system and the effect on the system [140, 141]. Such an approach allows the number of various cluster types to be increased. The frequency of the signals affecting nonautonomous systems can be changed and resonances resembling Arnold tongues for point 0-D systems observed [146].

Recently, the method of global negative feedback has been modified in terms of its locality. That is, the integrated global signal from the system is not taken; instead, the signal is obtained by averaging (or summing) over the system states only in some of its parts (locally – globally) [148 – 151]. This makes an intermediate variant between the global interaction of all system elements and the true local interaction via diffusion. Because variants of such local – global interactions are infinitely numerous, the appearance of new types of waves and patterns can be expected. Specifically, a new method to control localized trigger waves has been proposed [150].

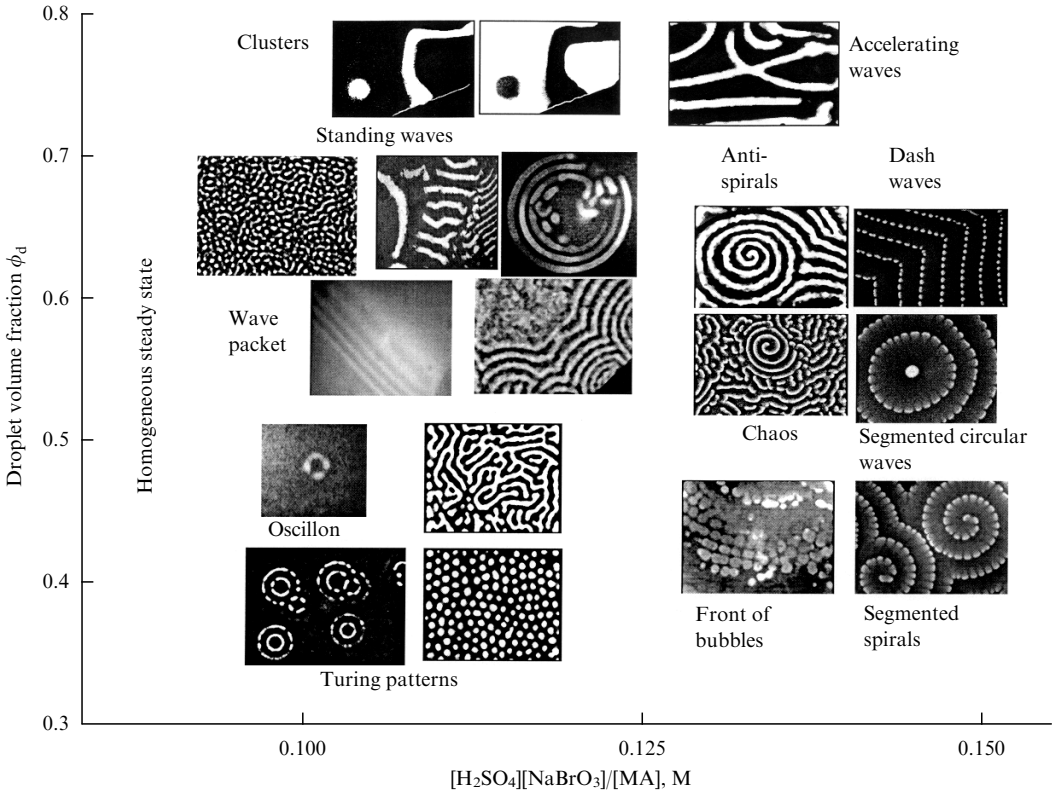

Figure 23. Summary table of patterns found in the BZ–AOT system. Stripe-like and circular standing waves are unstable and in the course of time evolve into spot-like standing waves shown among other standing waves in the left-hand part of the picture. There is only an arbitrary correspondence between the depicted structures and the axes of abscissas and ordinates.

10. Conclusion

To conclude, I present the table listing nonequilibrium patterns found in the BZ–AOT system (Fig. 23). No other experimental system has such a large variety of patterns. This allows the BZ–AOT reaction to be considered a useful and promising tool for studying pattern formation in reaction–diffusion systems. Some of the newly found nonequilibrium structures (such as segmented spirals or antispirals) have never been shown (or recognized) to occur in any biological or ecological system. Nevertheless, they might be helpful for understanding the behavior of certain real biological and physical objects.

NADP-H waves have recently been found in lymphocytes that do not annihilate upon collision [37, 38]. We have described packet waves having the same property. It is worthwhile to note that with the speed of packet waves being close to the phase velocity, the propagation of a solitary phase wave can be observed that is difficult to distinguish from that of a trigger wave at small distances. Certain microorganisms produce patterns reminiscent of segmented concentric waves [152]. The trajectories of separate segments of our segmented spiral are surprisingly similar to the structures found in a population of ameboid cells [36, 153]. This suggests the existence of cAMP segmented waves rather than smooth spiral ones in such cells. Chemical optics with attributes such as negative dispersion is consistent with recent discoveries in the theory of light propagation, e.g., negative refractive index and negative group velocity of light [154–156].

One of the promising lines of nonequilibrium pattern formation in reaction–diffusion systems is the interaction of these structures with the medium and the formation of new types of nonequilibrium patterns. Such a medium may be composed of 'soft materials', such as gels, microemulsions, and liquid crystals. It has been shown that the BZ reaction can alter the structure of these materials [157–159]; pH-oscillators can also periodically modify the structure of some materials (hydrogels) [160]. The theoretical basis for this line of developments is constituted by the works of Hildebrand, who has demonstrated that the interaction between thermodynamically stable nanostructures of size l and nonequilibrium concentration patterns having size L (dozens of millimeters) leads to the formation of new structures of size $(lL)^{1/2}$ [161–164]. In all likelihood, the BZ–AOT system may be suitable for studies directly related to the most puzzling aspects of the origin of life.

References

1. Field R J, Györgyi L (Eds) *Chaos in Chemistry and Biochemistry* (Singapore: World Scientific, 1993)
2. Ott E *Chaos in Dynamical Systems* (Cambridge: Cambridge Univ. Press, 1993)
3. Scott S K *Chemical Chaos* (Oxford: Clarendon Press, 1991)
4. Anishchenko V S *Slozhnye Kolebaniya v Prostykh Sistemakh* (Complex Oscillations in Simple Systems) (Moscow: Nauka, 1990)
5. Gammaitoni L et al. *Rev. Mod. Phys.* **70** 223 (1998)
6. Agladze K I, Krinsky V I *Nature* **296** 424 (1982)
7. Agladze K I et al. *Physica D* **39** 38 (1989)
8. Zaikin A N, Zhabotinsky A M *Nature* **225** 535 (1970)
9. Zhabotinskiĭ A M *Dokl. Akad. Nauk SSSR* **157** 392 (1964)
10. Field R J, Burger M (Eds) *Oscillations and Traveling Waves in Chemical Systems* (New York: Wiley, 1985)
11. Castets V et al. *Phys. Rev. Lett.* **64** 2953 (1990)
12. Turing A M *Philos. Trans. R. Soc. London Ser. B* **237** 37 (1952)

13. Gollub J P, Langer J S *Rev. Mod. Phys.* **71** s396 (1999)
14. Ivanitsky G R *Biofiz.* **44** 773 (1999) [*Biophys.* **44** 747 (1999)]
15. Ivanitskiĭ G R, Medvinskiĭ A B, Tsyganov M A *Usp. Fiz. Nauk* **164** 1041 (1994) [*Phys. Usp.* **37** 961 (1994)]
16. Jaeger H M, Nagel S R, Behringer R P *Rev. Mod. Phys.* **68** 1259 (1996)
17. Kerner B S, Osipov V V *Avtosolitony* (Autosolitons) (Moscow: Nauka, 1991)
18. Koch A J, Meinhardt H *Rev. Mod. Phys.* **66** 1481 (1994)
19. Medvinskiĭ A B et al. *Usp. Fiz. Nauk* **172** 31 (2002) [*Phys. Usp.* **45** 27 (2002)]
20. Merzhanov A G, Rumanov E N *Rev. Mod. Phys.* **71** 1173 (1999)
21. Mikhailov A S, Loskutov A Yu *Foundations in Synergetics II*: *Complex Patterns* 2nd ed. (Berlin: Springer, 1996)
22. Mikhailov A S, Hess B *J. Biol. Phys.* **28** 655 (2002)
23. Sagués F, Epstein I R *Dalton Trans.* (7) 1201 (2003)
24. Walgraef D *Spatio-Temporal Pattern Formation* (New York: Springer, 1996)
25. Mosekilde E, Mouritsen O G (Eds) *Modelling the Dynamics of Biological Systems*: *Nonlinear Phenomena and Pattern Formation* (Springer Ser. in Synergetics, Vol. 65) (Berlin: Springer, 1995)
26. Nicolis G *Introduction to Nonlinear Science* (Cambridge: Cambridge Univ. Press, 1995)
27. Arecchi F T, Boccaletti S, Ramazza P L *Phys. Rep.* **318** 1 (1999)
28. Taylor A F *Prog. React. Kinet. Mec.* **27** 247 (2002)
29. Larter R *J. Phys. Chem. B* **107** 415 (2003)
30. Borckmans P et al. *Int. J. Bifurcat. Chaos* **12** 2307 (2002)
31. De Wit A, in *Advances in Chemical Physics* Vol. 109 (Eds I Prigogine, S A Rice) (New York: J. Wiley, 1999) p. 435
32. Epstein I R, Pojman J A *An Introduction to Nonlinear Chemical Dynamics* (New York: Oxford Univ. Press, 1998)
33. Kapral R, Showalter K (Eds) *Chemical Waves and Patterns* (Understanding Chemical Reactivity, Vol. 10) (Dordrecht: Kluwer Acad. Publ., 1995)
34. Cross M C, Hohenberg P C *Rev. Mod. Phys.* **65** 851 (1993)
35. Epstein I R, Showalter K *J. Phys. Chem.* **100** 13132 (1996)
36. Ben-Jacob E, Cohen I, Levine H *Adv. Phys.* **49** 395 (2000)
37. Petty H R, Kindzelskii A L *Proc. Natl. Acad. Sci. USA* **98** 3145 (2001)
38. Kindzelskii A L, Petty H R *Proc. Natl. Acad. Sci. USA* **99** 9207 (2002)
39. Petty H R, Worth R G, Kindzelskii A L *Phys. Rev. Lett.* **84** 2754 (2000)
40. Petty H R, Kindzelskii A L *J. Phys. Chem. B* **104** 10952 (2000)
41. Lechleiter J et al. *Science* **252** 123 (1991)
42. Harris-White M E et al. *J. Neurophysiol.* **79** 1045 (1998)
43. Wu M, Ahlers G, Cannell D S *Phys. Rev. Lett.* **75** 1743 (1995)
44. Ecke R E et al. *Science* **269** 1704 (1995)
45. Astrov Yu A, Logvin Yu A *Phys. Rev. Lett.* **79** 2983 (1997)
46. Astrov Yu A et al. *Phys. Rev. Lett.* **80** 5341 (1998)
47. Coullet P, Riera C, Tresser C *Phys. Rev. Lett.* **84** 3069 (2000)
48. Umbanhowar P B, Melo F, Swinney H L *Nature* **382** 793 (1996)
49. Raizen M, Salomon C, Niu Q *Phys. Today* **50** (7) 30 (1997)
50. Schulman L S, Seiden P E *Science* **223** 425 (1986)
51. Guastello S J *Managing Emergent Phenomena*: *Nonlinear Dynamics in Work Organizations* (Mahwah, NJ: L. Erlbaum Associates, 2002)
52. Belousov B P, in *Sbornik Referatov po Radiatsionnoĭ Meditsine* (Collected Abstracts on Radiation Medicine) (Ed. A V Lebedinskiĭ) (Moscow: Medgiz, 1959) p. 145
53. Lengyel I, Rabai G, Epstein I R *J. Am. Chem. Soc.* **112** 4606 (1990)
54. De Kepper P et al. *J. Phys. Chem.* **86** 170 (1982)
55. Ertl G *Science* **254** 1750 (1991)
56. Mikhailov A S, Ertl G *Science* **272** 1596 (1996)
57. Mikhailov A S, Ertl G *Chaos* **12** 107 (2002)
58. Vanag V K, Boulanov D V *J. Phys. Chem.* **98** 1449 (1994)
59. Vanag V K, Hanazaki I *J. Phys. Chem.* **100** 10609 (1996)
60. Vanag V K, Hanazaki I *J. Phys. Chem. A* **101** 2147 (1997)
61. Vanag V K, Epstein I R *Phys. Rev. Lett.* **87** 228301 (2001)
62. Vanag V K, Epstein I R *Science* **294** 835 (2001)
63. Vanag V K, Epstein I R *Phys. Rev. Lett.* **88** 088303 (2002)
64. Vanag V K, Epstein I R *Phys. Rev. Lett.* **90** 098301 (2003)
65. Yeazell J, Uzer T (Eds) *The Physics and Chemistry of Wave Packets* (New York: Wiley, 2000)
66. Zhabotinsky A M, Dolnik M, Epstein I R *J. Chem. Phys.* **103** 10306 (1995)
67. Takagi S et al. *Phys. Rev. Lett.* **90** 124101 (2003)
68. Gray R A et al. *Phys. Rev. Lett.* **87** 168104 (2001)
69. Hamik C T, Manz N, Steinbock O *J. Phys. Chem. A* **105** 6144 (2001)
70. Hamik C T, Steinbock O *Phys. Rev. E* **65** 046224 (2002)
71. Vanag V K, Epstein I R *J. Phys. Chem. A* **106** 11394 (2002)
72. Kerner B S, Osipov V V *Autosolitons* (Dordrecht: Kluwer Acad., 1994)
73. Agladze K, Dulos E, De Kepper P *J. Phys. Chem.* **96** 2400 (1992)
74. Lengyel I, Epstein I R *Science* **251** 650 (1991)
75. Lengyel I, Epstein I R *Proc. Natl. Acad. Sci. USA* **89** 3977 (1992)
76. Ouyang Q, Swinney H L *Nature* **352** 610 (1991)
77. Rudovics B et al. *J. Phys. Chem. A* **103** 1790 (1999)
78. Vanag V K et al. *Nature* **406** 389 (2000)
79. Vanag V K, Zhabotinsky A M, Epstein I R *J. Phys. Chem. A* **104** 11566 (2000)
80. Vanag V K, Zhabotinsky A M, Epstein I R *Phys. Rev. Lett.* **86** 552 (2001)
81. Vanag V K, Epstein I R *Proc. Natl. Acad. Sci. USA* **100** 14635 (2003)
82. De T K, Maitra A *Adv. Colloid Interface Sci.* **59** 95 (1995)
83. Schwartz L J et al. *Langmuir* **15** 5461 (1999)
84. Lang J, Jada A, Malliaris A *J. Phys. Chem.* **92** 1946 (1988)
85. Baptista M S, Tran C D *J. Phys. Chem. B* **101** 4209 (1997)
86. Feldman Y et al. *J. Phys. Chem.* **100** 3745 (1996)
87. Mays H *J. Phys. Chem. B* **101** 10271 (1997)
88. Kurin-Csorgei K et al. *J. Phys. Chem. A* **101** 6827 (1997)
89. Gyorgyi L, Turanyi T, Field R J *J. Phys. Chem.* **94** 7162 (1990)
90. Vanag V K, Zhabotinsky A M, Epstein I R *J. Phys. Chem. A* **104** 8207 (2000)
91. Field R J, Koros E, Noyes R M *J. Am. Chem. Soc.* **94** 8649 (1972)
92. Field R J, Noyes R M *J. Chem. Phys.* **60** 1877 (1974)
93. Ciri R et al. *J. Phys. Chem. B* **103** 4997 (1999)
94. Keener J P, Tyson J J *Physica D* **21** 307 (1986)
95. Vasil'ev V A, Romanovskiĭ Yu M, Yakhno V G *Avtovolnovye Protsessy* (Autowave Processes) (Moscow: Nauka, 1987)
96. Vastano J A et al. *Phys. Lett. A* **124** 320 (1987)
97. Davies P W et al. *J. Phys. Chem. A* **102** 8236 (1998)
98. Roussel M R, Wang J *Phys. Rev. Lett.* **87** 188302 (2001)
99. Berenstein I et al. *Phys. Rev. Lett.* **91** 058302 (2003)
100. Dolnik M et al. *Phys. Rev. Lett.* **87** 238301 (2001)
101. Dolnik M, Zhabotinsky A M, Epstein I R *Phys. Rev. E* **63** 026101 (2001)
102. Horváth A K et al. *Phys. Rev. Lett.* **83** 2950 (1999)
103. Yang L, Epstein I R *Phys. Rev. Lett.* **90** 178303 (2003)
104. Mosekilde E et al. *Int. J. Bifurcat. Chaos* **8** 1003 (1998)
105. Gunaratne G H, Ouyang Q, Swinney H L *Phys. Rev. E* **50** 2802 (1994)
106. Zhou C, Guo H, Ouyang Q *Phys. Rev. E* **65** 036118 (2002)
107. Yang L et al. *Phys. Rev. Lett.* **88** 208303 (2002)
108. Shinbrot T et al. *Nature* **363** 411 (1993)
109. Nicolis G, Prigogine I *Self-Organization in Nonequilibrium Systems* (New York: Wiley, 1977)
110. Vanag V K, Epstein I R *J. Chem. Phys.* **119** 7297 (2003)
111. Herrero R et al. *Phys. Rev. Lett.* **84** 5312 (2000)
112. Holz R, Schneider F W *J. Phys. Chem.* **97** 12239 (1993)
113. Ramana Reddy D V, Sen A, Johnston G L *Phys. Rev. Lett.* **80** 5109 (1998)
114. Ramana Reddy D V, Sen A, Johnston G L *Phys. Rev. Lett.* **85** 3381 (2000)
115. von Oertzen A et al. *J. Phys. Chem. B* **104** 3155 (2000)
116. Yang L, Epstein I R *J. Phys. Chem. A* **106** 11676 (2002)
117. Stich M, Mikhailov A S *Z. Phys. Chem.* **216** 521 (2002)
118. Gong Y, Christini D J *Phys. Rev. Lett.* **90** 088302 (2003)
119. Mornev O A, Aslanidi O V, Chaĭlakhyan L M *Dokl. Ross. Akad. Nauk* **353** 682 (1997) [*Dokl. Biophys.* **352/354** 29 (1997)]
120. Mornev O A et al. *Pis'ma Zh. Eksp. Teor. Fiz.* **77** 319 (2003) [*JETP Lett.* **77** 270 (2003)]
121. Skødt H, Sørensen P G *Phys. Rev. E* **68** 020902(R) (2003)
122. Woo S-J, Lee J, Lee K J *Phys. Rev. E* **68** 016208 (2003)
123. Agladze K et al. *J. Phys. Chem.* **100** 13895 (1996)
124. Toth A, Gaspar V, Showalter K *J. Phys. Chem.* **98** 522 (1994)
125. Wellner M, Pertsov A M *Phys. Rev. E* **55** 7656 (1997)

126. Zykov V S *Biofiz*. **25** 888 (1980) [*Biophys*. **25** 906 (1980)]
127. Vanag V K, Hanazaki I *J. Phys. Chem*. **99** 6944 (1995)
128. Saunders P T (Ed.) *Morphogenesis* (Collected Works of A.M. Turing) (Amsterdam: North-Holland, 1992)
129. Vanag V K, Epstein I R *Phys. Rev. E* **67** 066219 (2003)
130. Lee K-J et al. *Nature* **369** 215 (1994)
131. Gray P, Scott S K *Chemical Oscillations and Instabilities*: *Non-linear Chemical Kinetics* (Oxford: Clarendon Press, 1990)
132. Schenk C P et al. *Phys. Rev. Lett*. **78** 3781 (1997)
133. Marsden J E, McCracken M *The Hopf Bifurcation and Its Applications* (New York: Springer-Verlag, 1976)
134. Strogatz S H *Nonlinear Dynamics and Chaos*: *With Applications to Physics, Biology, Chemistry, and Engineering* (Reading, Mass.: Addison-Wesley, 1994)
135. Jensen O et al. *Phys. Lett. A* **179** 91 (1993)
136. Jensen O et al. *Phys. Rev. E* **50** 736 (1994)
137. Vanag V K, Epstein I R *Phys. Rev. Lett*. **92** 128301 (2004)
138. Schuster S, Marhl M *J. Biol. Syst*. **9** 291 (2001)
139. Somogyi R, Stucki J W *J. Biol. Chem*. **266** 11068 (1991)
140. Bertram M, Mikhailov A S *Phys. Rev. E* **63** 066102 (2001)
141. Bertram M, Mikhailov A S *Phys. Rev. E* **67** 036207 (2003)
142. Bertram M et al. *Phys. Rev. E* **67** 036208 (2003)
143. Kim M et al. *Science* **292** 1357 (2001)
144. Kiss I Z, Zhai Y, Hudson J L *Science* **296** 1676 (2002)
145. Zykov V S, Mikhailov A S, Müller S C *Phys. Rev. Lett*. **78** 3398 (1997)
146. Lin A L et al. *Phys. Rev. Lett*. **84** 4240 (2000)
147. Petrov V, Ouyang Q, Swinney H L *Nature* **388** 655 (1997)
148. Hildebrand M, Skødt H, Showalter K *Phys. Rev. Lett*. **87** 088303 (2001)
149. Mihaliuk E et al. *Phys. Rev. E* **65** 065602(R) (2002)
150. Sakurai T et al. *Science* **296** 2009 (2002)
151. Wolff J et al. *Science* **294** 134 (2001)
152. Budrene E O, Berg H C *Nature* **376** 49 (1995)
153. Vasiev B N, Hogeweg P, Panfilov A V *Phys. Rev. Lett*. **73** 3173 (1994)
154. Cubukcu E et al. *Nature* **423** 604 (2003)
155. Foteinopoulou S, Economou E N, Soukoulis C M *Phys. Rev. Lett*. **90** 107402 (2003)
156. Wang L J, Kuzmich A, Dogariu A *Nature* **406** 277 (2000)
157. Dylla R J, Korgel B A *Chemphyschem* **2** (1) 62 (2001)
158. Kalishyn Y Yu et al. *Chem. Phys. Lett*. **363** 534 (2002)
159. Washington R P et al. *J. Am. Chem. Soc*. **121** 7373 (1999)
160. Dhanarajan A P, Misra G P, Siegel R A *J. Phys. Chem. A* **106** 8835 (2002)
161. Hildebrand M, Mikhailov A S, Ertl G *Phys. Rev. Lett*. **81** 2602 (1998)
162. Hildebrand M et al. *Phys. Rev. Lett*. **83** 1475 (1999)
163. Hildebrand M, Mikhailov A S *J. Stat. Phys*. **101** 599 (2000)
164. Hildebrand M et al. *New J. Phys*. **5** 61 (2003)
165. Agladze K I, Krinsky V I, Pertsov A M *Nature* **308** 834 (1984)